

# Numerical solution of two dimensional scalar conservation laws using compact implicit numerical schemes \*

Dagmar ŽÁKOVÁ<sup>1</sup> and Peter FROLKOVIČ<sup>2</sup>

<sup>1</sup>Department of Mathematics and Descriptive Geometry, Slovak University of Technology in Bratislava (dagmar.zakova@stuba.sk)

<sup>2</sup>Department of Mathematics and Descriptive Geometry, Slovak University of Technology in Bratislava (peter.frolkovic@stuba.sk)

**Abstract:** This paper deals with the numerical solution of conservation laws in the two dimensional case using a novel compact implicit time discretization that enable applications of fast algebraic solvers. We present details for the second order accurate parametric scheme based on the finite volume method including simple variants of ENO (Essentially Non-Oscillatory) and WENO (Weighted Essentially Non-Oscillatory) approximations. We present numerical experiments for representative linear and nonlinear problems.

**Key words:** conservation law, second order accuracy, compact implicit scheme, advection equation, Burgers equation

## 1 Introduction

Time dependent partial differential equations are typically solved by numerical methods where the time discretization is applied separately from the spatial discretization. Such an approach has the advantage that well developed and implemented numerical integration methods for the solutions of ordinary differential equations (ODEs) can be used after the equation is discretized in space. Already at the level of ODEs, it is recognized that the explicit type of time discretization methods are not suitable for systems of ODEs of which the solution describes processes with different time scales. In such a case, the restriction on the size of the time step of explicit schemes is no longer applicable if the fast processes require too small time steps only due to the stability constraints and not due to the accuracy requirements. A similar situation can occur when the time dependent solution in numerical simulations is approaching a stationary state, especially if some asymptotic preserving properties are expected from the numerical solution.

In the above mentioned cases, the well-known remedy is to apply implicit methods for the numerical solution of the ODEs that replace some explicit formulas to determine the numerical solution by discrete algebraic equations to be solved. This type of method is available with enhanced stability properties and offers, in an ideal case, the usage with the time steps having a size that is limited only by the accuracy requirements. The price to pay for such stability enhancement is strongly dependent on the efficiency with which the resulting discrete systems of algebraic equations can be solved.

Numerical methods based on the separate discretization of time and space have been well developed for hyperbolic systems. Concerning implicit methods (or their combinations with explicit methods), we can mention the class of Runge-Kutta (RK) methods used for hyperbolic problems in [20, 4, 12, 6, 1, 21, 19, 3, 22]. Furthermore, it is recognized that further improvements can be achieved if, opposite to standard RK methods, not only the values of the right hand side function are used, but also its derivatives. This approach is realized in the development of two- or multi-derivative RK methods [25, 27] available also in the form of implicit methods [29, 13]. Although all these methods are very well developed, their applications is not straightforward if some structure properties of the solution for hyperbolic equations shall be preserved not only by space discretization, but also by the time discretization.

The main idea of multi-derivative RK methods is shared with other types of time discretization methods that exploit finite Taylor series expansions of the solution with the so-called Lax-Wendroff (LW) or Cauchy-Kowalevskaya procedure when the time derivatives are replaced by corresponding derivatives of the right hand

---

\*The work was supported by the grants VEGA 1/0314/23, VEGA 1/0314/23 and APVV-19-0460.

side function. The methods based on the LW procedure offer a great opportunity to couple the time and space discretizations, so these methods can be developed in a hybrid way in which it can be easier to obtain some properties of numerical schemes. The simplest tool to realize it is to approximate each term in the Taylor series using different space discretizations [23, 25, 27, 16, 29]. The coupling of time and space discretization is strengthened in methods that use mixed spatial-temporal derivatives in the Lax-Wendroff procedure [31, 9, 5, 18].

As shown in [9, 11, 10], the idea of implicit time discretization using the LW procedure involving the mixed spatial-temporal derivatives can be used not only to enhance the stability of the method but also to improve the solvability of the resulting algebraic systems. In particular, a compact high-resolution finite difference method for hyperbolic problems in the one-dimensional case is presented in [10] in connection with the fractional step method [17] where the Jacobian matrix has a convenient structure, and therefore efficient solvers like the fast sweeping method [17] can be used.

In this work, we extend the approach of [10] in several aspects which indicate important steps towards applying the compact implicit scheme in even more general settings. The numerical scheme here is based on the two-dimensional finite volume method that offers more flexibility when, e.g., an extension for nonuniform grids is desired [26], while the finite difference method in [10] is tied up to uniform grids. In contrast to [17, 10], we do not use the fractional time step method, which can in many cases decrease accuracy of results due to time splitting errors [15]. To avoid unphysical oscillations, we propose high-resolution form of the compact implicit scheme using a Weighted Essentially Non-Oscillatory (WENO) reconstruction in space [26] not given in [10], and a nonlinear limiting in time using a flux limiter. Opposite to 1D case in [10], we treat here a space dependent velocity in 2D situations and relate the computations of parameters in the numerical scheme with theoretical results on a preservation of non-negative coefficients in the final numerical scheme. To further increase the efficiency of the method, we apply the predictor-corrector approach to compute the parameters in the WENO scheme as used in [21, 22]. We implement the fast sweeping method in the 2D case with proper orderings of unknowns in each Gauss-Seidel iteration to avoid a large number of iterations being used.

The main purpose of this study, similarly to [1, 21, 10], is to show that, following these guidelines, the resulting compact implicit scheme can be used for accurate numerical solutions of representative equations of scalar hyperbolic equations. The main motivation is to show that if the method is used as an implicit “black-box solver”, a good accuracy can be obtained in standard numerical experiments that is significantly improved with respect to the implicit first order accurate scheme. Consequently, the dominant criterion for the choice of time steps is the accuracy of numerical resolution for the solution phenomena that are of interest, and no restriction on the time step is required due to the stability requirement that might be related to some uninteresting phenomena. In this initial study, we do not compute numerical examples in which such stability requirements are presented, which we plan to do in our subsequent research.

The paper is organized as follows. In Section 2 we introduce the scalar conservation laws for two dimensional case and a general form of the finite volume method for its numerical solution. In Section 3 we derive a parametric form of a second order accurate scheme. In Section 4 we extend the schemes to the framework of a high resolution scheme with the use of the ENO (Essentially Non-Oscillatory) and WENO approximations. In Section 5 we illustrate the properties of the presented schemes with several numerical experiments and we conclude in Section 6. In Appendix, we present theoretical results for the discrete minimum and maximum principle in the case of linear advection equation with divergence free velocity.

## 2 Mathematical model and finite volume method

We consider two representative scalar hyperbolic partial differential equations in two-dimensional case. First, we consider the nonlinear hyperbolic equation in the form

$$\partial_t u + \nabla \cdot \mathbf{f}(u) = 0, \quad (1)$$

with  $\mathbf{f}(u) = (f(u), g(u))$  being the vector flux function, so (1) can be written in the form

$$\partial_t u + \partial_x f(u) + \partial_y g(u) = 0 \quad (2)$$

with  $u = u(x, y, t)$  being the unknown function for  $t \in (0, T)$  and  $x \in (x_L, x_R) \subset R$ ,  $y \in (y_L, y_R) \subset R$ . The initial condition is defined by  $u(x, y, 0) = u^0(x, y)$  and the Dirichlet boundary conditions, if prescribed, are denoted by

$$u(x_L, y, t) = u_{x_L}(y, t), \quad u(x, y_L, t) = u_{y_L}(x, t), \quad u(x_R, y, t) = u_{x_R}(y, t), \quad u(x, y_R, t) = u_{y_R}(x, t). \quad (3)$$

Next, we introduce the numerical discretization to solve the equation (2). The discretization is done in space and time using the following notation. We denote  $t^n = n\tau$ ,  $n = 0, 1, \dots, N$  for a chosen  $N$  and  $\tau > 0$  with  $t^{n+1/2} = t^n + \tau/2$ . The spatial discretization is based on the finite volume method [8, 15, 2]. For simplicity of the notation, we assume a squared computational domain that is divided into finite volumes of the form  $I_{i,j} = (x_{i-1/2}, x_{i+1/2}) \times (y_{j-1/2}, y_{j+1/2})$  with the regular square grid, where  $x_{i-1/2} = x_L + ih - h/2$  and  $y_{j-1/2} = x_L + jh - h/2$  with  $i, j = 1, 2, \dots, M$  for the chosen  $M$  and  $h = (x_R - x_L)/M$ .

The main idea behind the finite volume method is to integrate the differential equation (2) over  $I_{i,j} \times (t^n, t^{n+1})$

$$\int_{t^n}^{t^{n+1}} \int_{I_{i,j}} (\partial_t u + \partial_x f(u) + \partial_y g(u)) dx dy dt = 0. \quad (4)$$

Using the divergence theorem with  $n(s) = (n^x(s), n^y(s))$  be the outward-pointing unit normal vector to the boundary  $\partial I_{i,j}$  of the finite volume  $I_{i,j}$  at a point  $(x(s), y(s))$ , we can express

$$\begin{aligned} \int_{I_{i,j}} (\partial_x f(u) + \partial_y g(u)) dx dy &= \int_{\partial I_{i,j}} (n^x(s)f(u) + n^y(s)g(u)) ds \\ &= \int_{y_{j-1/2}}^{y_{j+1/2}} f(u(x_{i+1/2}, y, t)) dy - \int_{y_{j-1/2}}^{y_{j+1/2}} f(u(x_{i-1/2}, y, t)) dy \\ &\quad + \int_{x_{i-1/2}}^{x_{i+1/2}} g(u(x, y_{j+1/2}, t)) dx - \int_{x_{i-1/2}}^{x_{i+1/2}} g(u(x, y_{j-1/2}, t)) dx. \end{aligned} \quad (5)$$

Next, using the notation for the space and time averaged values defined as

$$\begin{aligned} \tilde{u}_{i,j}^n &:= \frac{1}{h^2} \int_{I_{i,j}} u(x, y, t^n) dx dy, \\ f_{i+1/2,j} &:= \frac{1}{\tau h} \int_{t^n}^{t^{n+1}} \int_{y_{j-1/2}}^{y_{j+1/2}} f(u(x_{i+1/2}, y, t)) dy dt, \\ g_{i,j+1/2} &:= \frac{1}{\tau h} \int_{t^n}^{t^{n+1}} \int_{x_{i-1/2}}^{x_{i+1/2}} g(u(x, y_{j+1/2}, t)) dx dt, \end{aligned} \quad (6)$$

one can rewrite (4) to the equivalent form,

$$\tilde{u}_{i,j}^{n+1} - \tilde{u}_{i,j}^n + \frac{\tau}{h} (f_{i+1/2,j} - f_{i-1/2,j}) + \frac{\tau}{h} (g_{i,j+1/2} - g_{i,j-1/2}) = 0. \quad (7)$$

To obtain a numerical scheme from (7), one has to approximate the integrals in (6). As we aim to obtain the second order accuracy, we consider midpoint quadrature rules. Using  $u_{i,j}^n \approx \tilde{u}_{i,j}^n \approx u(x_i, y_j, t^n)$ ,  $F_{i+1/2,j} \approx f_{i+1/2,j} \approx f(u(x_{i+1/2}, y_j, t^{n+1/2}))$ ,  $G_{i,j+1/2} \approx g_{i,j+1/2} \approx g(u(x_i, y_{j+1/2}, t^{n+1/2}))$ , the numerical scheme takes then the form

$$u_{i,j}^{n+1} - u_{i,j}^n + \frac{\tau}{h} (F_{i+1/2,j} - F_{i-1/2,j}) + \frac{\tau}{h} (G_{i,j+1/2} - G_{i,j-1/2}) = 0. \quad (8)$$

To construct the numerical fluxes, we follow standard approaches [26, 15, 7] of proposing approximations  $u_{i+1/2,j}^{n+1/2,\pm} \approx u(x_{i+1/2}, y_j, t^{n+1/2})$  and  $u_{i,j+1/2}^{n+1/2,\pm} \approx u(x_i, y_{j+1/2}, t^{n+1/2})$  that correspond to numerical values obtained by linear reconstructions in related finite volumes, namely  $u_{i+1/2,j}^{n+1/2,-}$  in  $I_{i,j}$  and  $u_{i+1/2,j}^{n+1/2,+}$  in  $I_{i+1,j}$ , and analogously for  $u_{i,j+1/2}^{n+1/2,\pm}$ . Having such values and properly chosen flux function  $H = H(u^-, u^+)$  of two arguments [26, 15], one defines

$$F_{i+1/2,j} = H(u_{i+1/2,j}^{n+1/2,-}, u_{i+1/2,j}^{n+1/2,+}), \quad (9)$$

and similarly for the flux  $G_{i,j+1/2}$ ,

$$G_{i,j+1/2} = H(u_{i,j+1/2}^{n+1/2,-}, u_{i,j+1/2}^{n+1/2,+}), \quad (10)$$

*PF presuniam do experimentov* For our purposes, we choose the Godunov flux  $H$  defined by

$$H(u^-, u^+) = \begin{cases} \min_{u^- \leq u \leq u^+} h(u) & \text{if } u^- \leq u^+ \\ \max_{u^+ \leq u \leq u^-} h(u) & \text{if } u^- > u^+ \end{cases} \quad (11)$$

where  $h = f$  for (9) and  $h = g$  for (10).

Defining in the first step the notation of finite volume methods for the nonlinear scalar equation, in the second step we give additional details for the two dimensional linear advection equation with variable velocity. Here, the flux function  $\mathbf{f}$  in (1) is formally represented by  $\mathbf{f} = \vec{v}u$  with a given space dependent velocity field  $\vec{v} = \vec{v}(x, y) = (v(x, y), w(x, y))$ . The flux function  $\mathbf{f}$  now depends on the space variables that we consider only for the linear advection, so the problem (1) takes the form

$$\partial_t u + \partial_x(vu) + \partial_y(wu) = 0. \quad (12)$$

In this case, the numerical fluxes are defined as follows,

$$\begin{aligned} F_{i+1/2,j} &= v_{i+1/2,j}^+ u_{i+1/2,j}^{n+1/2,-} + v_{i+1/2,j}^- u_{i+1/2,j}^{n+1/2,+}, \\ G_{i,j+1/2} &= w_{i,j+1/2}^+ u_{i,j+1/2}^{n+1/2,-} + w_{i,j+1/2}^- u_{i,j+1/2}^{n+1/2,+}, \end{aligned} \quad (13)$$

where

$$v_{i\pm 1/2,j} := v(x_{i\pm 1/2}, y_j), \quad w_{i,j\pm 1/2} := w(x_i, y_{j\pm 1/2}). \quad (14)$$

and we applied the splitting of the velocity vector field,

$$\begin{aligned} v &= v^+ + v^-, & \text{with } v^+ &:= \max(0, v), \quad v^- := \min(0, v), \\ w &= w^+ + w^-, & \text{with } w^+ &:= \max(0, w), \quad w^- := \min(0, w), \end{aligned} \quad (15)$$

In summary, the numerical scheme (8) will transform into the form

$$\begin{aligned} u_{i,j}^{n+1} - u_{i,j}^n &+ \frac{\tau}{h} (v_{i+1/2,j}^+ u_{i+1/2,j}^{n+1/2,-} - v_{i-1/2,j}^+ u_{i-1/2,j}^{n+1/2,-}) + \frac{\tau}{h} (w_{i,j+1/2}^+ u_{i,j+1/2}^{n+1/2,-} - w_{i,j-1/2}^+ u_{i,j-1/2}^{n+1/2,-}) \\ &+ \frac{\tau}{h} (v_{i+1/2,j}^- u_{i+1/2,j}^{n+1/2,+} - v_{i-1/2,j}^- u_{i-1/2,j}^{n+1/2,+}) + \frac{\tau}{h} (w_{i,j+1/2}^- u_{i,j+1/2}^{n+1/2,+} - w_{i,j-1/2}^- u_{i,j-1/2}^{n+1/2,+}) = 0. \end{aligned} \quad (16)$$

Note that the simplest first order accurate numerical scheme uses the approximations

$$\begin{aligned} u_{i+1/2,j}^{n+1/2,-} &= u_{i,j}^{n+1}, & u_{i+1/2,j}^{n+1/2,+} &= u_{i+1,j}^{n+1}, \\ u_{i,j+1/2}^{n+1/2,-} &= u_{i,j}^{n+1}, & u_{i,j+1/2}^{n+1/2,+} &= u_{i,j+1}^{n+1}. \end{aligned} \quad (17)$$

### 3 The second order accurate parametric compact implicit scheme

In this section, we present the parametric form of the second order accurate scheme in time and space that is later used also in the framework of high resolution schemes. As discussed above, one has to define the approximations  $u_{i+1/2,j}^{n+1/2,\pm}$  and  $u_{i,j+1/2}^{n+1/2,\pm}$  based on the upwind approach. For simplicity of the derivation, we will treat in detail only the derivation for the values  $u_{i+1/2,j}^{n+1/2,-}$  and  $u_{i,j+1/2}^{n+1/2,-}$ . Similarly, one can handle the values  $u_{i+1/2,j}^{n+1/2,+}$  and  $u_{i,j+1/2}^{n+1/2,+}$  for which we will present only the final definitions.

To approximate the values  $u_{i+1/2,j}^{n+1/2,-}$  and  $u_{i,j+1/2}^{n+1/2,-}$  up to the second order of accuracy [7], we apply a finite Taylor series,

$$u(x_{i+1/2}, y_j, t^{n+1/2}) = u(x_i, y_j, t^{n+1}) + \frac{h}{2} \partial_x u(x_i, y_j, t^{n+1}) - \frac{\tau}{2} \partial_t u(x_i, y_j, t^{n+1}) + \mathcal{O}(h^2, \tau^2) \quad (18)$$

and

$$u(x_i, y_{j+1/2}, t^{n+1/2}) = u(x_i, y_j, t^{n+1}) + \frac{h}{2} \partial_y u(x_i, y_j, t^{n+1}) - \frac{\tau}{2} \partial_t u(x_i, y_j, t^{n+1}) + \mathcal{O}(h^2, \tau^2). \quad (19)$$

Similarly to [7], we do not replace the time derivative using the Lax-Wendroff procedure, but we approximate (18) and (19) directly. Formally, the desired numerical values would then be defined as

$$\begin{aligned} u_{i+1/2,j}^{n+1/2,-} &= u_{i,j}^{n+1} + \frac{h}{2} \partial_x u_{i,j}^{n+1} - \frac{\tau}{2} \partial_t u_{i,j}^{n+1}, \\ u_{i,j+1/2}^{n+1/2,-} &= u_{i,j}^{n+1} + \frac{h}{2} \partial_y u_{i,j}^{n+1} - \frac{\tau}{2} \partial_t u_{i,j}^{n+1}, \end{aligned} \quad (20)$$

where the approximations  $\partial_x u_{i,j}^{n+1}$ ,  $\partial_y u_{i,j}^{n+1}$  and  $\partial_t u_{i,j}^{n+1}$  we express differently to [7], namely as a linear combination of two different approximation choices [10] using parameters  $\omega \in [0, 1]$ , namely,

$$\begin{aligned} u_{i+1/2,j}^{n+1/2,-} &= u_{i,j}^{n+1} + \frac{1}{2}(\omega^{x,-}(u_{i,j}^{n+1} - u_{i-1,j}^{n+1}) + (1 - \omega^{x,-})(u_{i+1,j}^{n+1} - u_{i,j}^{n+1})) \\ &\quad - \frac{1}{2}(\omega^{x,-}(u_{i,j}^{n+1} - u_{i,j}^n) + (1 - \omega^{x,-})(u_{i+1,j}^{n+1} - u_{i+1,j}^n)) \\ &= u_{i,j}^{n+1} - \frac{1}{2}(\omega^{x,-}(u_{i-1,j}^{n+1} - u_{i,j}^n) + (1 - \omega^{x,-})(u_{i,j}^{n+1} - u_{i+1,j}^n)), \end{aligned} \quad (21)$$

$$\begin{aligned} u_{i,j+1/2}^{n+1/2,-} &= u_{i,j}^{n+1} + \frac{1}{2}(\omega^{y,-}(u_{i,j}^{n+1} - u_{i,j-1}^{n+1}) + (1 - \omega^{y,-})(u_{i,j+1}^{n+1} - u_{i,j}^{n+1})) \\ &\quad - \frac{1}{2}(\omega^{y,-}(u_{i,j}^{n+1} - u_{i,j}^n) + (1 - \omega^{y,-})(u_{i,j+1}^{n+1} - u_{i,j+1}^n)) \\ &= u_{i,j}^{n+1} - \frac{1}{2}(\omega^{y,-}(u_{i,j-1}^{n+1} - u_{i,j}^n) + (1 - \omega^{y,-})(u_{i,j}^{n+1} - u_{i,j+1}^n)). \end{aligned} \quad (22)$$

Notice that we have managed to obtain a compact stencil as the values  $u_{i+1,j}^{n+1}$  and  $u_{i,j+1}^{n+1}$  in (21) and (22) are canceled. This is also the substantial difference to the approach given in [7]. Two particular choices of parameters  $\omega^{x,-} \in [0, 1]$  and  $\omega^{y,-} \in [0, 1]$  do not use the full stencil in (21) and (22) that we use later conveniently for ENO approximation [26]. In particular, with the value  $\omega^{x,-} = 0$  and  $\omega^{y,-} = 0$  we create in (21) and (22) a "central" kind of discretization and for  $\omega^{x,-} = 1$  (and  $\omega^{y,-} = 1$ ) the "upwind" one.

Very similarly, one obtains the numerical approximations of  $u_{i+1/2,j}^{n+1/2,+}$  and  $u_{i,j+1/2}^{n+1/2,+}$  as

$$\begin{aligned} u_{i+1/2,j}^{n+1/2,+} &= u_{i+1,j}^{n+1} - \frac{1}{2}(\omega^{x,+}(u_{i+2,j}^{n+1} - u_{i+1,j}^n) + (1 - \omega^{x,+})(u_{i+1,j}^{n+1} - u_{i,j}^n)), \\ u_{i,j+1/2}^{n+1/2,+} &= u_{i,j+1}^{n+1} - \frac{1}{2}(\omega^{y,+}(u_{i,j+2}^{n+1} - u_{i,j+1}^n) + (1 - \omega^{y,+})(u_{i,j+1}^{n+1} - u_{i,j}^n)). \end{aligned} \quad (23)$$

We gather all parameters by  $\omega = (\omega^{x,\pm}, \omega^{y,\pm})$ . Note that the parameters can be different in each grid node and time point, which we do not emphasize here in the notation.

To finalize the second order accurate compact implicit scheme, we express the numerical fluxes in (8) using (9) and (10) with the numerical approximations  $u_{i+1/2,j}^{n+1/2,\pm}$ ,  $u_{i,j+1/2}^{n+1/2,\pm}$  from (21), (22), and (23). The approach presented here is used in [28] to extend the accuracy further in the 1D case up to the third order for smooth solutions with the help of fractional step method. In that case, one has to use the Lax-Wendroff procedure with mixed derivatives of the solution [31, 9, 5] to preserve the compactness of the scheme.

The discretization scheme creates a system of algebraic equations that can be solved iteratively using the fast sweeping method, where each sweeping iteration is given by one (linear or nonlinear) Gauss-Seidel iteration applied sequentially with alternating index directions across the computational domain [30, 17]. In particular, we use four different "sweeps" from each corner of a rectangular domain:

$$\begin{aligned} i &= 1, \dots, M, \quad j = 1, \dots, M \\ i &= M, \dots, 1, \quad j = 1, \dots, M \\ i &= M, \dots, 1, \quad j = M, \dots, 1 \\ i &= 1, \dots, M, \quad j = M, \dots, 1 \end{aligned} \quad (24)$$

where each *sweep* represents the Gauss-Seidel method (GS) with the given ordering. Note that in the case of a nonlinear flux function  $\mathbf{f}$ , one has to solve a scalar nonlinear algebraic equation for each pair of indices  $i$  and  $j$  in the sweeps as other unknowns are given in the manner of Gauss-Seidel iterations. When solving the linear advection equation (12) with a constant velocity, the solution of the system of algebraic equations can be obtained by performing only one particular sweep in (24). In general, more than four Gauss-Seidel sweep iterations (4GS) shall be used for each time step that we document in numerical experiments. Nevertheless, we observe the second order accuracy of numerical solutions for chosen examples with smooth solutions even after 4GS.

## 4 High resolution schemes

For discontinuous initial conditions or when shocks are present in the solution of (2), unphysical oscillations may occur in numerical solutions if the numerical methods from the previous section with fixed parameters are

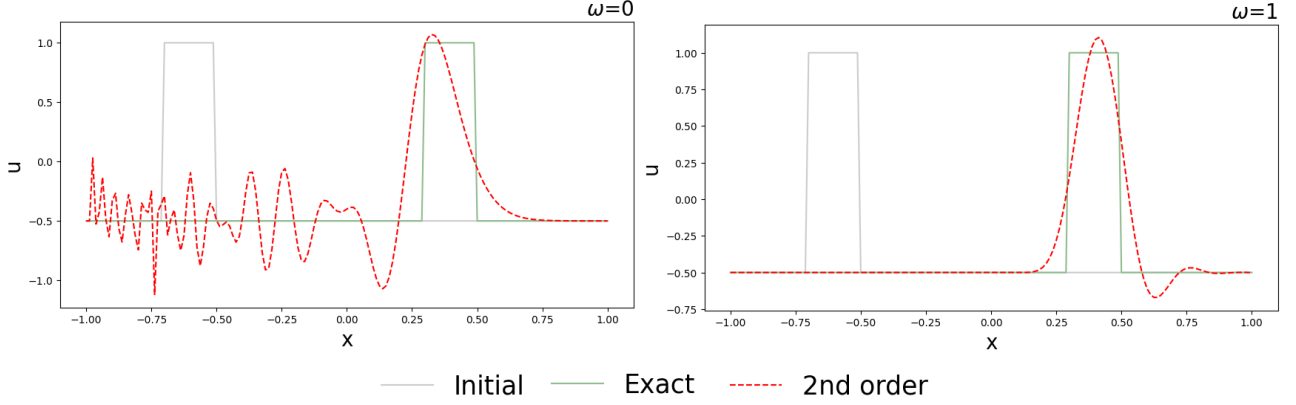


Figure 1: Cross-sectional views of a numerical solutions of a linear advection equation, with the discontinuous initial condition, obtained using the second order accurate scheme and the fixed choices of  $\omega^{x,\pm}, \omega^{y,\pm} = 0, 1$ , sequentially, at each  $I_{i,j}$ . The Courant number equals 5. For the description of the example see the section 5 on numerical experiments.

used, as illustrated in Figure 1. To avoid such oscillations, we choose the values of the parameters  $\omega$  in each numerical flux differently, i.e., depending on the numerical solution [26, 10].

Let  $\omega^{x,\pm} = \omega_{i,j}^{x,\pm} \in [0, 1]$  and  $\omega^{y,\pm} = \omega_{i,j}^{y,\pm} \in [0, 1]$  for each  $I_{i,j}$  in (21) and (22) be the free parameters that we want to determine. As is known from the literature [7, 1, 21, 10, 22], unphysical oscillations can occur not only due to an inappropriately fixed choice of space reconstruction, but also due to the fixed time reconstruction. Therefore, similarly to [10], we add another numerical parameter  $\mathbf{l} = (l^{x,\pm}, l^{y,\pm})$ , which, if necessary, can limit the second order space reconstruction to the first order form of the scheme that produces numerical solutions free of unphysical oscillations. Again, the parameter  $\mathbf{l}$  is defined in each  $I_{i,j}$  in the form  $l^{x,\pm}, l^{y,\pm} \in [0, 1]$ . Notice that the values  $\omega$  and  $\mathbf{l}$  also change at each time step, which we do not emphasize in the notation.

In summary, the approximation (21) and (22) will transform into the form

$$\begin{aligned} u_{i+1/2,j}^{n+1/2,-} &= u_{i,j}^{n+1} - \frac{l_{i,j}^{x,-}}{2} (\omega_{i,j}^{x,-} (u_{i-1,j}^{n+1} - u_{i,j}^n) + (1 - \omega_{i,j}^{x,-}) (u_{i,j}^{n+1} - u_{i+1,j}^n)), \\ u_{i,j+1/2}^{n+1/2,-} &= u_{i,j}^{n+1} - \frac{l_{i,j}^{y,-}}{2} (\omega_{i,j}^{y,-} (u_{i,j-1}^{n+1} - u_{i,j}^n) + (1 - \omega_{i,j}^{y,-}) (u_{i,j}^{n+1} - u_{i,j+1}^n)), \end{aligned} \quad (25)$$

and for (23)

$$\begin{aligned} u_{i+1/2,j}^{n+1/2,+} &= u_{i+1,j}^{n+1} - \frac{l_{i+1,j}^{x,+}}{2} (\omega_{i+1,j}^{x,+} (u_{i+2,j}^{n+1} - u_{i+1,j}^n) + (1 - \omega_{i+1,j}^{x,+}) (u_{i+1,j}^{n+1} - u_{i,j}^n)), \\ u_{i,j+1/2}^{n+1/2,+} &= u_{i,j+1}^{n+1} - \frac{l_{i,j+1}^{y,+}}{2} (\omega_{i,j+1}^{y,+} (u_{i,j+2}^{n+1} - u_{i,j+1}^n) + (1 - \omega_{i,j+1}^{y,+}) (u_{i,j+1}^{n+1} - u_{i,j}^n)). \end{aligned} \quad (26)$$

The high-resolution scheme is then defined by (8) - (11) with the interface values given in (25) - (26).

Concerning the space reconstruction, we present in the next sections two standard choices - the simplest Essentially Non-Oscillatory (ENO) method and a variant of the Weighted ENO (WENO) method. The value of  $\omega$  for the ENO method will depend on the following ratios in  $\mathbf{r} = (r_{i,j}^{x,\pm}, r_{i,j}^{y,\pm})$ ,

$$\begin{aligned} r_{i,j}^{x,-} &= \frac{u_{i-1,j}^{n+1} - u_{i,j}^n}{u_{i,j}^{n+1} - u_{i+1,j}^n}, & r_{i,j}^{x,+} &= \frac{u_{i+1,j}^{n+1} - u_{i,j}^n}{u_{i,j}^{n+1} - u_{i-1,j}^n}, \\ r_{i,j}^{y,-} &= \frac{u_{i,j-1}^{n+1} - u_{i,j}^n}{u_{i,j}^{n+1} - u_{i,j+1}^n}, & r_{i,j}^{y,+} &= \frac{u_{i,j+1}^{n+1} - u_{i,j}^n}{u_{i,j}^{n+1} - u_{i,j-1}^n}, \end{aligned} \quad (27)$$

while the WENO method will depend on the nominators and denominators in the definitions of  $\mathbf{r}$ . Clearly, due to the dependence of  $\mathbf{r}$  on unknown values of numerical solution, an iterative procedure shall be proposed to compute the parameters  $\omega$ . We present later a predictor-corrector method as proposed in [21, 10].

Once the solution dependent values of  $\omega$  are computed, they are used for the definition of the parameters

$l_{i,j}^{x,-}, l_{i,j}^{y,-}$  that are determined by

$$\begin{aligned} l_{i,j}^{x,-} &= \min \left\{ 1, \max \left\{ 0, \left( \omega_{i,j}^{x,-} + \frac{1 - \omega_{i,j}^{x,-}}{r_{i,j}^{x,-}} \right)^{-1} \left( \frac{2}{C} + l_{i-1,j}^{x,-} (\omega_{i-1,j}^{x,-} r_{i-1,j}^{x,-} + 1 - \omega_{i-1,j}^{x,-}) \right) \right\} \right\}, \\ l_{i,j}^{y,-} &= \min \left\{ 1, \max \left\{ 0, \left( \omega_{i,j}^{y,-} + \frac{1 - \omega_{i,j}^{y,-}}{r_{i,j}^{y,-}} \right)^{-1} \left( \frac{2}{C} + l_{i,j-1}^{y,-} (\omega_{i,j-1}^{y,-} r_{i,j-1}^{y,-} + 1 - \omega_{i,j-1}^{y,-}) \right) \right\} \right\}, \end{aligned} \quad (28)$$

and similarly for  $l_{i,j}^{x,+}, l_{i,j}^{y,+}$ . Here, the parameter  $C$  is the local Courant like number. For the nonlinear scalar equation, the parameter  $C$  is defined analogously to the treatment in the 1D case as presented in [10],

$$C = \max \left\{ 1, \frac{\tau}{h} \max_u |f'(u)| + \frac{\tau}{h} \max_u |g'(u)| \right\}. \quad (29)$$

However, the linear advection equation in the 2D case with variable velocity must be treated with more care. In Appendix, we derive the conditions under which the numerical scheme (16) with (25) and (26) for divergence free velocity fields, i.e.,  $\nabla \cdot \vec{v} = 0$ , produces numerical solutions fulfilling discrete minimum and maximum principle. These conditions also motivate the definitions of (28) for this case.

In the following subsections, we present the simplest ENO and WENO procedures adapted to our compact implicit numerical scheme.

#### 4.1 ENO procedure

With an appropriate choice of  $\omega_{i,j}^{x,\pm}, \omega_{i,j}^{y,\pm}$  being either 0 or 1, we can define the Essentially Non-Oscillatory (ENO) scheme [26]. The choice can be based on the parameters  $\mathbf{r}$  in (27),

$$\begin{aligned} \omega_{i,j}^{x,-} &= \begin{cases} 1 & \text{if } |r_{i,j}^{x,-}| \leq 1 \\ 0 & \text{otherwise} \end{cases}, & \omega_{i,j}^{x,+} &= \begin{cases} 1 & \text{if } |r_{i,j}^{x,+}| \leq 1 \\ 0 & \text{otherwise} \end{cases}, \\ \omega_{i,j}^{y,-} &= \begin{cases} 1 & \text{if } |r_{i,j}^{y,-}| \leq 1 \\ 0 & \text{otherwise} \end{cases}, & \omega_{i,j}^{y,+} &= \begin{cases} 1 & \text{if } |r_{i,j}^{y,+}| \leq 1 \\ 0 & \text{otherwise} \end{cases}. \end{aligned} \quad (30)$$

To evaluate the nonlinear dependence on  $u_{i,j}^{n+1}$ , the predictor-corrector procedure is used in the following steps:

1. Calculate a predicted value  $u_{i,j}^{n+1}$  using the numerical scheme (8) - (11) and (21) - (23) with the fixed values  $\omega_{i,j}^{x,\pm} = \omega_{i,j}^{y,\pm} = 0$ . The calculation involves performing (at least) four Gauss-Seidel (4GS) sweep iterations (24).
2. The corrector step consists of (at least) 4GS iterations in the prescribed order (24), where for each of the iterations, one needs to perform:
  - 2.1 Calculate  $r_{i,j}^{x,\pm}$  and  $r_{i,j}^{y,\pm}$  from (27) using the predicted value of  $u_{i,j}^{n+1}$ .
  - 2.2 Set  $\omega_{i,j}^{x,\pm}$  and  $\omega_{i,j}^{y,\pm}$  with (30) based on the calculated  $\mathbf{r}$  in the step 2.1; afterwards, calculate the values  $l_{i,j}^{x,\pm}, l_{i,j}^{y,\pm}$  from (28).
  - 2.3 Calculate the corrected value  $u_{i,j}^{n+1}$  using the obtained values  $\omega_{i,j}^{x,\pm}, \omega_{i,j}^{y,\pm}$  and  $l_{i,j}^{x,\pm}$  and  $l_{i,j}^{y,\pm}$  in the step 2.2.
  - 2.4 Set either the corrected value as a new predictor and perform again the Step 2, or accept the corrected values.

We compute several numerical experiments (see Section 5) with the ENO scheme for which we investigate, among others, the behavior of the fast sweeping method depending on the number of Gauss-Seidel iterations.

#### 4.2 WENO procedure

To create a weighted essentially non-oscillatory scheme, we propose, again, a solution-dependent choice of  $\omega_{i,j}^{x,\pm}, \omega_{i,j}^{y,\pm}$  as found in [26] and adapted to our compact implicit scheme. The WENO scheme is used to achieve a smoother choice, comparing to the ENO scheme, between the „upwind” and „central” differences in (21) - (22) and (23), so  $\omega_{i,j}^{x,\pm}, \omega_{i,j}^{y,\pm} \in [0, 1]$ .

Let  $\bar{\omega}$  be some preferable constant value of  $\omega_{i,j}^{x,\pm}, \omega_{i,j}^{y,\pm}$ , e.g.  $\bar{\omega} = 1/3$  to achieve the third accurate approximation of  $\partial_x u$  in (20). Then, using the nominators and denominators in  $\mathbf{r}$  given in (27), we set firstly the weights

$$\begin{aligned} a_u^{x,-} &= \bar{\omega} \left( \frac{1}{(\epsilon + (u_{i-1,j}^{n+1} - u_{i,j}^n)^2)^2} \right), & a_u^{y,-} &= \bar{\omega} \left( \frac{1}{(\epsilon + (u_{i,j-1}^{n+1} - u_{i,j}^n)^2)^2} \right), \\ a_c^{x,-} &= (1 - \bar{\omega}) \left( \frac{1}{(\epsilon + (u_{i,j}^{n+1} - u_{i+1,j}^n)^2)^2} \right), & a_c^{y,-} &= (1 - \bar{\omega}) \left( \frac{1}{(\epsilon + (u_{i,j}^{n+1} - u_{i,j+1}^n)^2)^2} \right), \end{aligned} \quad (31)$$

and

$$\begin{aligned} a_u^{x,+} &= \bar{\omega} \left( \frac{1}{(\epsilon + (u_{i+1,j}^{n+1} - u_{i,j}^n)^2)^2} \right), & a_u^{y,+} &= \bar{\omega} \left( \frac{1}{(\epsilon + (u_{i,j+1}^{n+1} - u_{i,j}^n)^2)^2} \right), \\ a_c^{x,+} &= (1 - \bar{\omega}) \left( \frac{1}{(\epsilon + (u_{i,j}^{n+1} - u_{i-1,j}^n)^2)^2} \right), & a_c^{y,+} &= (1 - \bar{\omega}) \left( \frac{1}{(\epsilon + (u_{i,j}^{n+1} - u_{i,j-1}^n)^2)^2} \right), \end{aligned} \quad (32)$$

with  $\epsilon$  being a small number to avoid a zero division. Afterwards, we can construct the parameters  $\omega_{i,j}^{x,\pm}, \omega_{i,j}^{y,\pm}$  by

$$\omega_{i,j}^{x,-} = \frac{a_u^{x,-}}{a_u^{x,-} + a_c^{x,-}}, \quad \omega_{i,j}^{y,-} = \frac{a_u^{y,-}}{a_u^{y,-} + a_c^{y,-}}, \quad \omega_{i,j}^{x,+} = \frac{a_u^{x,+}}{a_u^{x,+} + a_c^{x,+}}, \quad \omega_{i,j}^{y,+} = \frac{a_u^{y,+}}{a_u^{y,+} + a_c^{y,+}}. \quad (33)$$

The corrector-predictor procedure for using the WENO scheme is composed of the following steps:

1. Calculate a predicted value  $u_{i,j}^{n+1}$ , using the numerical scheme with the given starting value  $\omega_{i,j}^{x,\pm} = \omega_{i,j}^{y,\pm} = \bar{\omega}$ . The calculation involves performing the fast sweeping method.
2. The corrector step consists of (at least) 4GS iterations in the prescribed order as given in (24), where for each of the iterations, one needs to perform:
  - 2.1 Calculate the weights  $a_{u,c}^{x,\pm}, a_{u,c}^{y,\pm}$  from (31 - 32) using the predicted value.
  - 2.2 Set  $\omega_{i,j}^{x,\pm}, \omega_{i,j}^{y,\pm}$  with (33) using the weights from the previous step; get the values  $l_{i,j}^{x,\pm}, l_{i,j}^{y,\pm}$  from (28).
  - 2.3 Calculate the corrected value  $u_{i,j}^{n+1}$  using the obtained values  $\omega_{i,j}^{x,\pm}, \omega_{i,j}^{y,\pm}$  and  $l_{i,j}^{x,\pm}, l_{i,j}^{y,\pm}$ .
  - 2.4 Set either the corrected value as a new predictor and perform again the Step 2, or accept the corrected values.

## 5 Numerical experiments

We present numerical results of the proposed second order and high resolution compact implicit finite-volume scheme with the purpose of illustrating their accuracy and stability properties. We describe the results in two subsections, the first one dealing with a linear advection equation, and the second one dealing with the Burgers equation as a simple representative nonlinear problem. For each of the cases, we present an example with a smooth initial condition, as well as an example with a discontinuous initial condition, employing both the ENO and WENO scheme. Specifically for the Burgers equation, we demonstrate two phenomena, shock and rarefaction waves, separately.

If the exact solution is known for the chosen example, it is used for boundary conditions, and the discrete  $L_1$  norm ( $E$ ) of the error is calculated as follows,

$$E = h^2 \sum_{i=1}^M \sum_{j=1}^M |u_{ij}^N - \bar{u}_{ij}^N|. \quad (34)$$

Moreover, the Experimental Order of Convergence (EOC) is computed using the errors from (34) to confirm the expected order of the accuracy for the chosen examples. Note that to avoid a reduction of the accuracy due to boundary conditions when computing the EOC, we set exact values not only at the inflow boundary points, but also in a neighboring point outside of the computational interval to use the full stencil of the scheme for every inner grid point. Concerning the time steps, we choose maximal Courant numbers larger than allowed by a stability restriction of explicit schemes. In such a way, we document a stable behavior of the unconditionally



stable compact implicit schemes by preserving satisfactory accuracy. As the chosen examples do not contain any stiff features, if only the accuracy is considered, they can be solved better by explicit type of schemes. Nevertheless, our primary purpose is to show that no significant loss of the accuracy is observed when applying large time steps that is in a large contrast with the unconditionally stable first order accurate implicit scheme.

The numerical methods and the graphical output are obtained using the Python programming language [24].

## 5.1 Linear advection equation

First, we compute the linear advection equation given in (12). As a guiding factor to compare the results, we compute the maximal value of Courant number at each direction,

$$C_{max}^x = \frac{\tau}{h} \max_{i,j} \{|v_{i+1/2,j}|\}, \quad C_{max}^y = \frac{\tau}{h} \max_{i,j} \{|w_{i,j+1/2}|\},$$

over all edges of each finite volume. These "directional" Courant numbers will be larger than allowed by a stability restriction of explicit schemes. Note that the Courant like number  $C$  in (28), to define the parameters 1 to "limit in time", are defined by

$$C = C_{i+1/2,j}^{x,+} - C_{i-1/2,j}^{x,-} + C_{i,j+1/2}^{y,+} - C_{i,j-1/2}^{y,-}, \quad (35)$$

with

$$\begin{aligned} C_{i+1/2,j}^{x,+} &= \frac{\tau}{h} v_{i+1/2,j}^+, & C_{i-1/2,j}^{x,-} &= \frac{\tau}{h} v_{i-1/2,j}^-, \\ C_{i,j+1/2}^{y,+} &= \frac{\tau}{h} w_{i,j+1/2}^+, & C_{i,j-1/2}^{y,-} &= \frac{\tau}{h} w_{i,j-1/2}^-, \end{aligned} \quad (36)$$

see also the Appendix for the motivation.

We choose the computation domain  $x, y \in [-1, 1]$  and the velocity field representing the rotation in the form

$$\vec{v} = (-2\pi y, 2\pi x), \quad (37)$$

which is shown in Figure 2, where the exact solution for any initial function  $u^0$  is defined as

$$u(x, y, t) = u^0(x \cos(2\pi t) + y \sin(2\pi t), y \cos(2\pi t) - x \sin(2\pi t)). \quad (38)$$

In the first example, we consider the initial condition in a form of Gaussian,

$$u^0(x, y) = e^{10(-(x-0.25)^2 - (y-0.25)^2)} \quad (39)$$

and in the first experiment, we will choose the final time  $T = 0.25$ . In such a case, the Gaussian moves by a quarter of a cycle. The initial function with the exact solution are shown in Fig. 3.

We compute the experiment for three different (but fixed) choices of  $\omega$  to show the second order accuracy of the method.

We choose sequentially  $M = 40, 80, 160, 320$  and  $640$ , and  $N = M/10$  which leads to  $C_{max}^x = C_{max}^y = 7.854$ . The initial condition together with the contours of the numerical solution are shown in Fig. 5 for different times  $t = T/3, 2T/3, T$ , with  $T = 0.25$ . The errors and the EOCs in Table 1 confirm the expected order of accuracy for the three different pairs of values  $\omega^{x,\pm}, \omega^{y,\pm} = 0, 1/2, 1$  used. We also apply the ENO and WENO ( $\bar{\omega} = 1/3$ ) schemes to check the order of accuracy for such schemes. We also compute the errors and the EOCs using the first order accurate numerical scheme (17) to show the significant difference in the errors when using the higher order accurate schemes. For this first experiment, to solve the system of linear algebraic equations, a fast sweeping method with four Gauss-Seidel iterations sufficed.

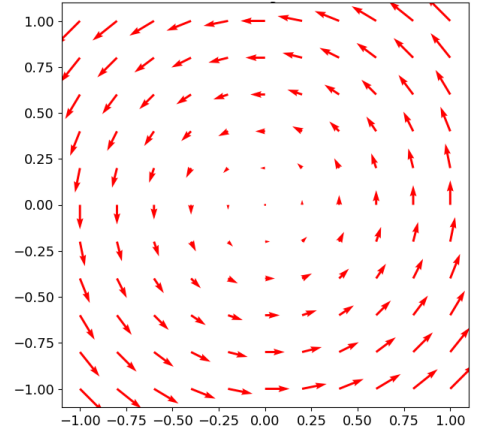


Figure 2: Velocity field in (37).

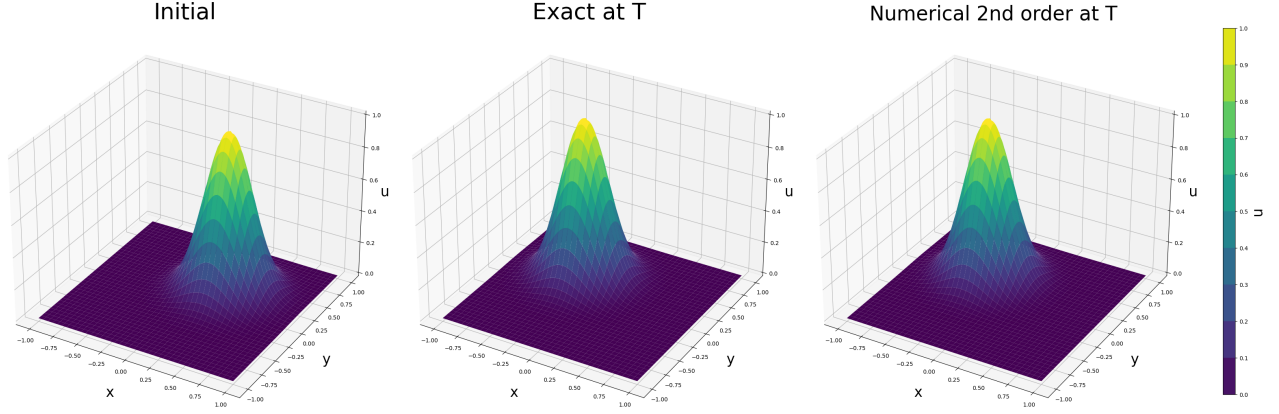


Figure 3: The initial condition, the exact solution and the numerical solution obtained by the second order accurate scheme with  $\omega^{x,\pm}, \omega^{y,\pm} = 0$ ,  $M = 320$ ,  $T = 0.25$ , only 4 Gauss-Seidel iterations are performed.

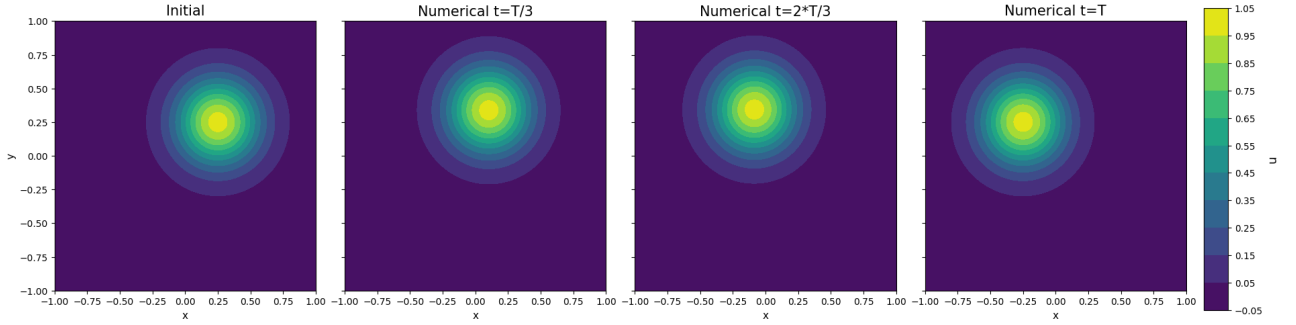


Figure 4: Contours of the numerical solution of the rotation of Gaussian, obtained by the second order accurate scheme with 4GS and  $\omega^{x,\pm}, \omega^{y,\pm} = 0$  at different times  $t = 0, T/3, 2T/3, T$  with  $M = 320$ , and with  $C_{max}^x = C_{max}^y = 7.854$ .

Next, we present numerical results for a non-smooth solution. As an initial condition for  $x, y \in [-1, 1]$ , we choose four formations in four quadrants, see (40) and Fig. 6. In particular, a Gaussian with the center at  $(0.5, 0.5)$  and the height equals 1; a cone with the center at  $(-0.5, 0.5)$  with the maximal radius  $r_{max} = 0.25$  and the height 1; a half sphere with the center at  $(-0.5, -0.5)$  and the maximal radius  $r_{max}$  and the height 1; and a circle with a center at  $(0.5, -0.5)$  with radius  $r_{max}$  with the value 1 inside the circle and the value 0 everywhere else.

$$u^0(x, y) = \begin{cases} e^{100(-(x-0.5)^2-(y-0.5)^2)} & \text{if } x \geq 0 \text{ and } y \geq 0 \text{ and } (x-0.5)^2 + (y-0.5)^2 < 0.3^2, \\ 1 - \frac{\sqrt{(x+0.5)^2+(y-0.5)^2}}{0.25} & \text{if } x < 0 \text{ and } y \geq 0 \text{ and } \sqrt{(x+0.5)^2 + (y-0.5)^2} \leq 0.25, \\ \sqrt{1 - \left(\frac{\sqrt{(x+0.5)^2+(y+0.5)^2}}{0.25}\right)^2} & \text{if } x < 0 \text{ and } y < 0 \text{ and } \sqrt{(x+0.5)^2 + (y+0.5)^2} \leq 0.25, \\ 1 & \text{if } x \geq 0 \text{ and } y < 0 \text{ and } \sqrt{(x-0.5)^2 + (y+0.5)^2} \leq 0.25, \\ 0 & \text{otherwise.} \end{cases} \quad (40)$$

The velocity field is the same as in (37), and we choose the final time  $T = 0.25$ . The exact solution is obtained using (38). The initial condition and the final solution are shown in Figure 6. We choose  $M = 40, 80, 160, 320, 640$  and  $N = M/10$  time steps, leading to  $C_{max}^x = C_{max}^y = 7.854$ .

This time, it is necessary to use the ENO and WENO ( $\bar{\omega} = 1/3$ ) schemes to suppress oscillations in numerical solutions. The errors and the EOCs are shown in Table 2 for the entire computational domain. The differences in the errors for 4 and 8 GS iterations are shown to show rather negligible differences. The Table also contains the comparison to the errors when using the first order accurate scheme. Moreover, in Table 3, the errors and the EOCs are displayed for each sector separately, showing the convergence of each of the formations in the initial condition using the 4 and 8 GS iterations.

		$\omega^{x,\pm}, \omega^{y,\pm} = 0$			$\omega^{x,\pm}, \omega^{y,\pm} = 1/2$			$\omega^{x,\pm}, \omega^{y,\pm} = 1$		
$M$	$N$	E	EOC	max	E	EOC	max	E	EOC	max
40	4	0.06959	-	0.95	0.03687	-	0.95	0.02543	-	0.93
80	8	0.02163	1.68	0.97	0.01087	1.76	0.99	0.00693	1.92	0.98
160	16	0.00578	1.90	0.99	0.00285	1.93	0.99	0.00175	1.98	0.99
320	32	0.00147	1.97	0.99	0.00072	1.98	0.99	0.00043	1.99	0.99
640	64	0.00037	1.99	0.99	0.00018	1.99	0.99	0.00010	1.99	0.99

		ENO			WENO			1st order		
$M$	$N$	E	EOC	max	E	EOC	max	E	EOC	max
40	4	0.04917	-	0.81	0.04513	-	0.84	0.15530	-	0.58
80	8	0.01594	1.62	0.91	0.01604	1.49	0.97	0.10447	0.57	0.69
160	16	0.00491	1.69	0.96	0.00472	1.76	0.98	0.06366	0.71	0.80
320	32	0.00136	1.85	0.98	0.00125	1.91	0.99	0.03600	0.82	0.88
640	64	0.00036	1.88	0.99	0.00032	1.95	0.99	0.01932	0.89	0.93

Table 1: The numerical errors and the EOCs of the second order schemes for the rotation of Gaussian,  $C_{max}^x = C_{max}^y = 7.854$ .

		ENO, 4GS		WENO, 4GS		ENO, 8GS		WENO, 8GS		1st order	
$M$	$N$	E	EOC	E	EOC	E	EOC	E	EOC	E	EOC
40	4	0.48031	-	0.45872	-	0.47765	-	0.45959	-	0.56302	-
80	8	0.32450	0.56	0.30956	0.56	0.32022	0.57	0.29833	0.62	0.53127	0.08
160	16	0.18626	0.80	0.18315	0.75	0.18285	0.80	0.17129	0.80	0.45594	0.22
320	32	0.10187	0.87	0.10120	0.85	0.09987	0.87	0.09414	0.86	0.35630	0.35
640	64	0.05768	0.82	0.05749	0.81	0.05624	0.83	0.05353	0.81	0.25809	0.46

Table 2: The numerical errors and the EOCs for the ENO and WENO schemes, the example of the rotation of a discontinuous function (40) with  $T = 0.25$  over entire computational domain,  $C_{max}^x = C_{max}^y = 7.854$ .

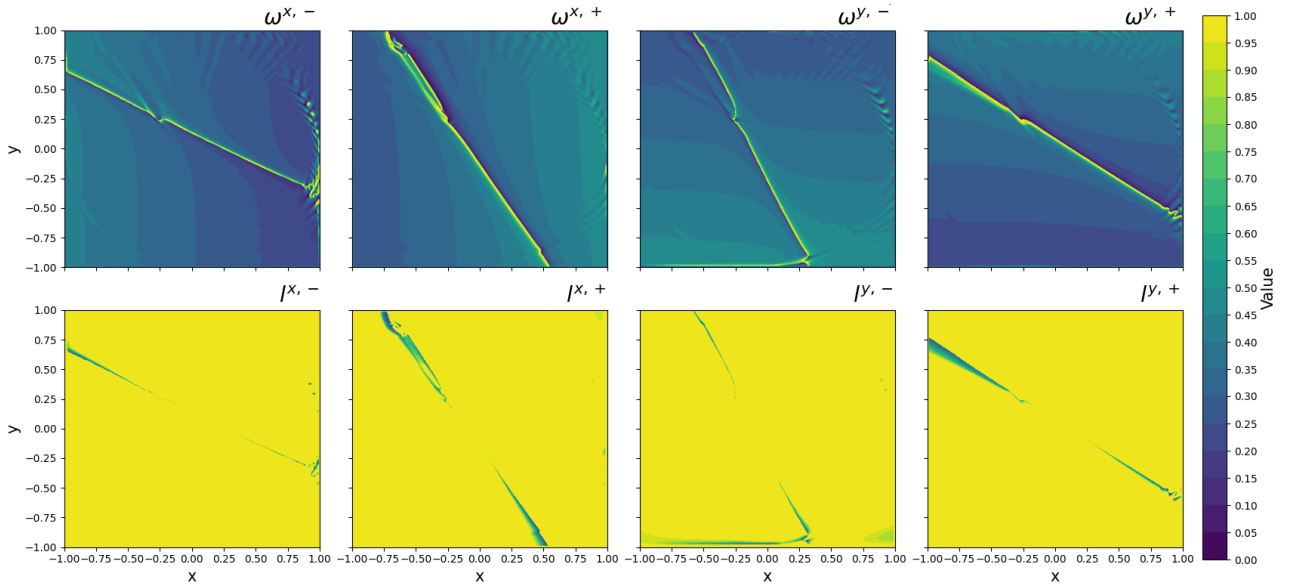


Figure 5: Visualization of  $\omega$  and  $l$  at the final time  $T = 0.25$  when using the WENO scheme with 4GS and  $\bar{\omega} = 1/3$  for the rotation of Gaussian,  $M = 320$ ,  $C_{max}^x = C_{max}^y = 7.854$ .

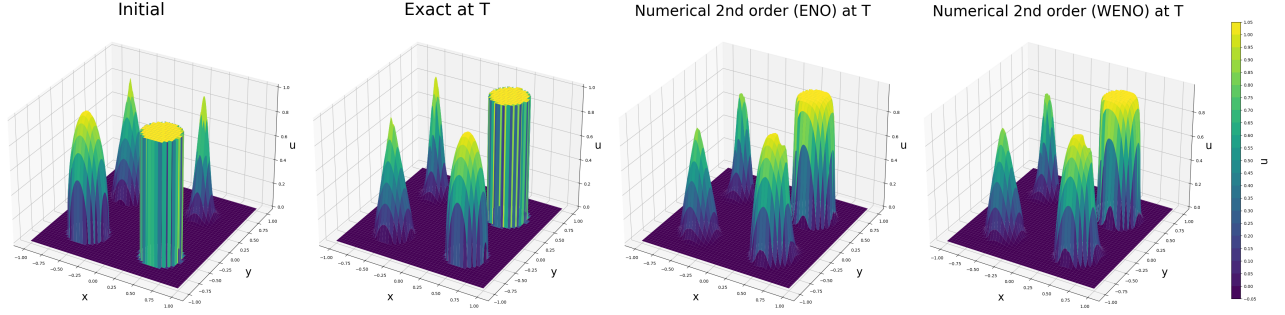


Figure 6: The initial condition and the exact solution for the example of the rotation of (40) with  $M = 640$ , and numerical results using the ENO and WENO schemes with 8GS.

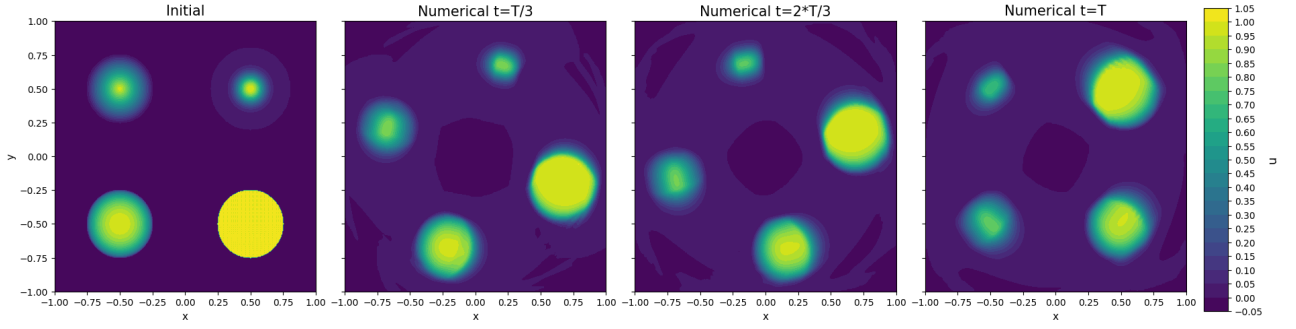


Figure 7: The numerical solution for the example of the rotation of (40) at three times  $t = 0, T/3, 2T/3, T$  and  $T = 0.25$  obtained using the ENO (8GS) scheme,  $M = 320$ ,  $C_{max}^x = C_{max}^y = 7.854$ .

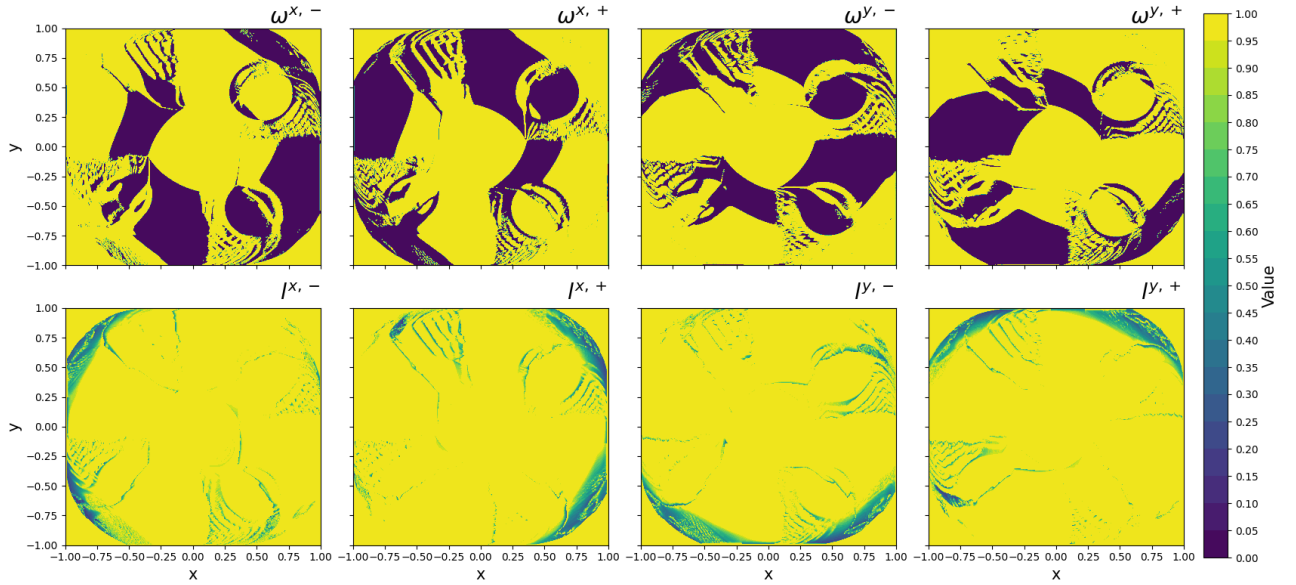


Figure 8: The visualizations of the values of  $\omega$  and  $l$  at  $T = 0.25$  obtained using the ENO (8GS) scheme for the rotation of (40),  $M = 320$ ,  $C_{max}^x = C_{max}^y = 7.854$ .

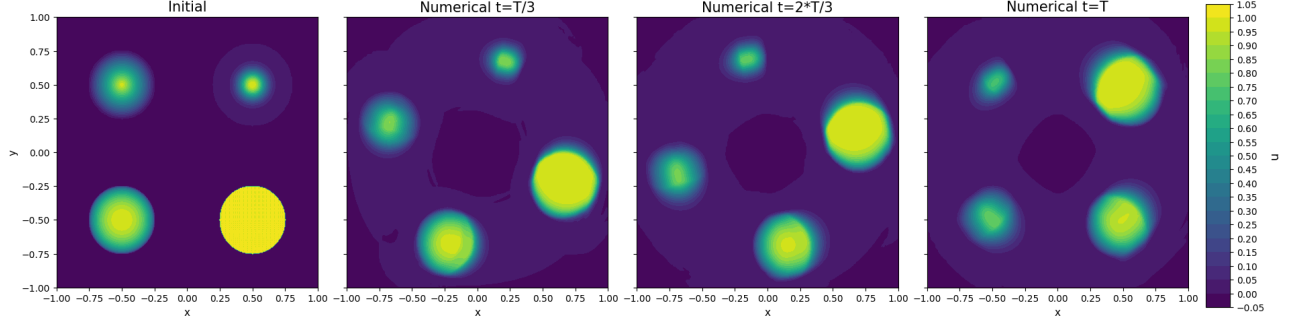


Figure 9: The numerical solution for the example of the rotation of (40) at three times  $t = 0, T/3, 2T/3, T$  and  $T = 0.25$  obtained using the WENO (8GS) scheme,  $M = 320$ ,  $C_{max}^x = C_{max}^y = 7.854$ .

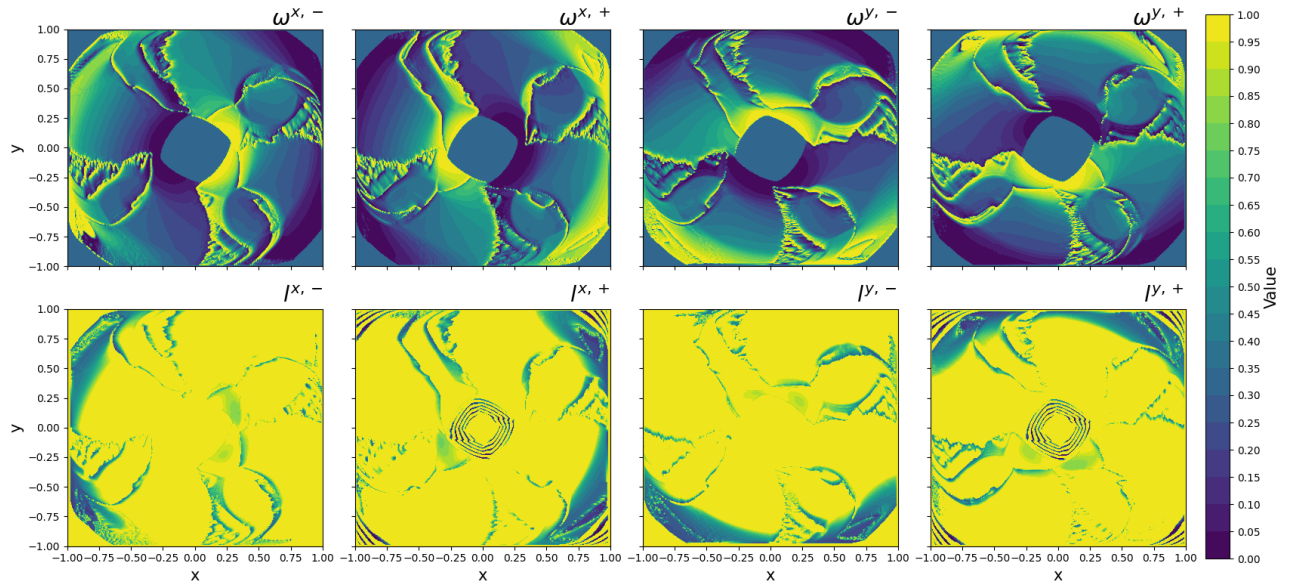


Figure 10: The visualizations of the values of  $\omega$  and  $l$  at  $T = 0.25$  obtained using the WENO (8GS) scheme for the rotation of (40),  $M = 320$ ,  $C_{max}^x = C_{max}^y = 7.854$ .

ENO, 4GS									
		Gaussian		Cone		Half sphere		Circle	
$M$	$N$	E	EOC	E	EOC	E	EOC	E	EOC
80	8	0.03482	-	0.04953	-	0.09152	-	0.09152	-
160	16	0.01985	0.81	0.02453	1.01	0.04660	0.97	0.04660	0.64
320	32	0.00924	1.10	0.00989	1.31	0.02229	1.06	0.02229	0.65
640	64	0.00378	1.28	0.00408	1.27	0.01170	0.92	0.01170	0.66
WENO, 4GS									
		Gaussian		Cone		Half sphere		Circle	
$M$	$N$	E	EOC	E	EOC	E	EOC	E	EOC
80	8	0.03345	-	0.05008	-	0.08574	-	0.14028	-
160	16	0.02041	0.71	0.02651	0.91	0.04503	0.92	0.09118	0.62
320	32	0.01008	1.01	0.01080	1.29	0.02203	1.03	0.05827	0.64
640	64	0.00424	1.24	0.00454	1.24	0.01177	0.90	0.03692	0.65
ENO, 8GS									
		Gaussian		Cone		Half sphere		Circle	
$M$	$N$	E	EOC	E	EOC	E	EOC	E	EOC
80	8	0.03456	-	0.04850	-	0.09029	-	0.14686	-
160	16	0.01955	0.82	0.02371	1.00	0.04601	0.97	0.09356	0.65
320	32	0.00902	1.11	0.00960	1.30	0.02222	1.04	0.05901	0.66
640	64	0.00365	1.30	0.00396	1.27	0.01171	0.92	0.03691	0.68
WENO, 8GS									
		Gaussian		Cone		Half sphere		Circle	
$M$	$N$	E	EOC	E	EOC	E	EOC	E	EOC
80	8	0.04764	-	0.04600	-	0.08303	-	0.13693	-
160	16	0.01846	0.80	0.02277	1.01	0.04201	0.98	0.08804	0.63
320	32	0.00867	1.08	0.00937	1.28	0.02040	1.04	0.05569	0.66
640	64	0.00386	1.16	0.00398	1.23	0.01086	0.90	0.03482	0.68

Table 3: The numerical errors and the EOCs for the ENO and WENO schemes, each quadrant separately, the example of the rotation of (40) with  $T = 0.25$ ,  $C_{max}^x = C_{max}^y = 7.854$ .

## 5.2 Burgers equation

We compute a representative nonlinear problem in the form of the Burgers equation,

$$\partial_t u + \partial_x \left( \frac{u^2}{2} \right) + \partial_y \left( \frac{u^2}{2} \right) = 0. \quad (41)$$

In this case, the maximum Courant number is defined as  $C_{max} = \frac{\tau}{h} u_{max}$ , with  $u_{max} = \max(|u_{i,j}^n|)$  over all time steps and finite volumes.

For the first 2D example we choose the computation domain  $x, y \in [-1, 1]$  and  $t \in [0, 0.5]$  with a smooth initial condition (Fig. 11) in the form

$$u^0(x, y) = \sin(\pi x) \sin(\pi y) / 2. \quad (42)$$

The exact solution can be obtained numerically using the method of characteristics by solving the algebraic equations for  $u = u(x_i, y_j, t^n)$

$$u = \sin(\pi(x_i - ut^n)) \sin(\pi(y_j - ut^n)) / 2. \quad (43)$$

For this example, we chose sequentially  $M = 80, 160, 320$  and  $640$ , and the number of time steps is  $N = M/80$ . Together with the maximum absolute value of the function  $u^0$  being  $0.5$ , one obtains  $C_{max} = 10$ .

We show results using the compact implicit numerical scheme with the constant values of  $\omega^{x,\pm}, \omega^{y,\pm} = 0, 1/2, 1$ , sequentially. We compute the errors (34) in the final time  $T = 0.5$ , the EOC and also the minimum and maximum value of  $u$ . The errors and the EOCs in Table 4 confirm the expected order of accuracy for the different values  $\omega^{x,\pm}, \omega^{y,\pm}$ . We also show results using the ENO and WENO (with  $\bar{\omega} = 1/3$ ) schemes, to demonstrate the order of accuracy. Notice that the maximum and minimum values when using the ENO and WENO schemes keep the values of  $u$  within the limits, unlike the constant value of  $\omega$  used everywhere else. The results can be compared with the errors of the first order accurate scheme in Table 4. The visualization of the choice of  $\omega$  and  $l$  for the ENO and WENO schemes are shown in Figures 13, 14, respectively.

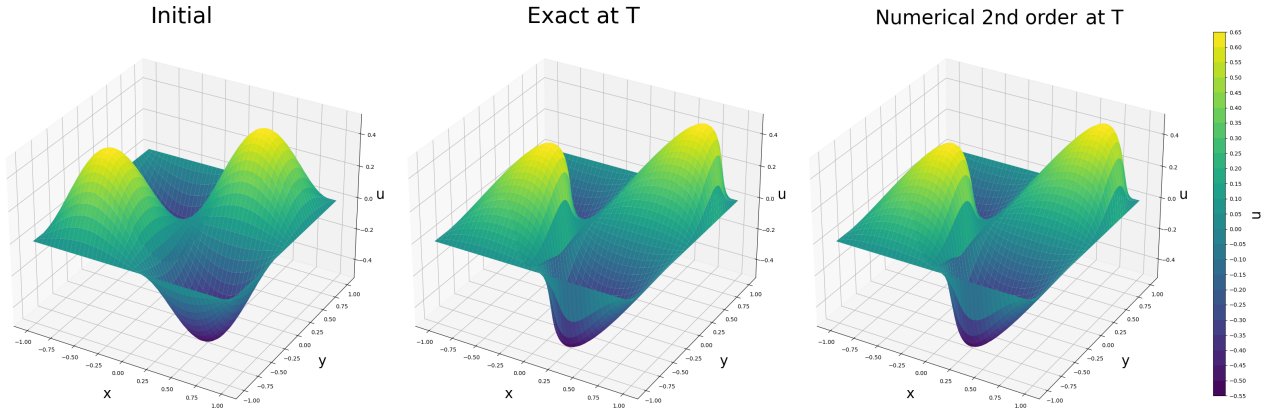


Figure 11: The initial condition (left), the exact solution (middle) and the numerical solution (right) obtained by the second order scheme at  $T = 0.5$  using 4GS for the nonlinear problem with the smooth initial condition (42),  $\omega^{x,\pm}, \omega^{y,\pm} = 1$ ,  $M = 320$ .



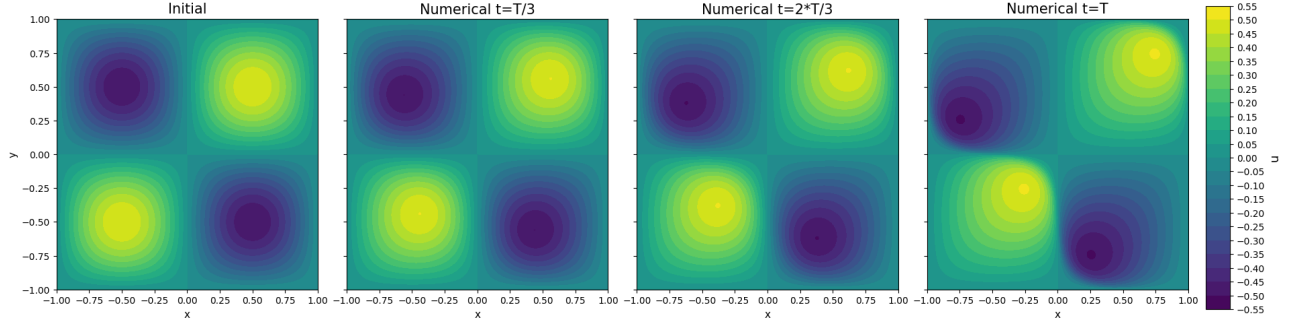


Figure 12: Contours of the numerical solution of the nonlinear problem with the smooth initial condition (42) obtained by the second order accurate numerical scheme (4GS) at times  $t = 0, T/3, 2T/3, T$  with  $T = 0.5$ ,  $M = 320$ ,  $\omega^{x,\pm}, \omega^{y,\pm} = 1$ ,  $C_{max} = 10$ .

		$\omega^{x,\pm}, \omega^{y,\pm} = 0$				$\omega^{x,\pm}, \omega^{y,\pm} = 1/2$				$\omega^{x,\pm}, \omega^{y,\pm} = 1$			
$M$	$N$	E	EOC	min	max	E	EOC	min	max	E	EOC	min	max
80	1	0.0599	-	-0.510	0.510	0.0516	-	-0.508	0.508	0.0436	-	-0.503	0.503
160	2	0.0247	1.27	-0.505	0.505	0.0209	1.29	-0.504	0.504	0.0175	1.31	-0.506	0.506
320	4	0.0083	1.56	-0.501	0.501	0.0069	1.59	-0.501	0.501	0.0057	1.61	-0.503	0.503
640	8	0.0024	1.78	-0.500	0.500	0.0019	1.80	-0.500	0.500	0.0016	1.83	-0.501	0.501

		ENO				WENO				1st order			
$M$	$N$	E	EOC	min	max	E	EOC	min	max	E	EOC	min	max
80	1	0.0603	-	-0.460	0.460	0.0590	-	-0.460	0.460	0.1323	-	-0.417	0.417
160	2	0.0255	1.23	-0.478	0.478	0.0250	1.23	-0.477	0.477	0.0918	0.52	-0.433	0.433
320	4	0.0082	1.63	-0.489	0.489	0.0080	1.62	-0.489	0.489	0.0595	0.62	-0.453	0.453
640	8	0.0023	1.83	-0.497	0.496	0.0022	1.82	-0.496	0.496	0.0357	0.73	-0.470	0.470

Table 4: The numerical errors, the EOCs and the minimum and maximum values for the first and second order schemes computed for the nonlinear problem with the smooth initial condition (42),  $T = 0.5$ ,  $C_{max} = 10$ .

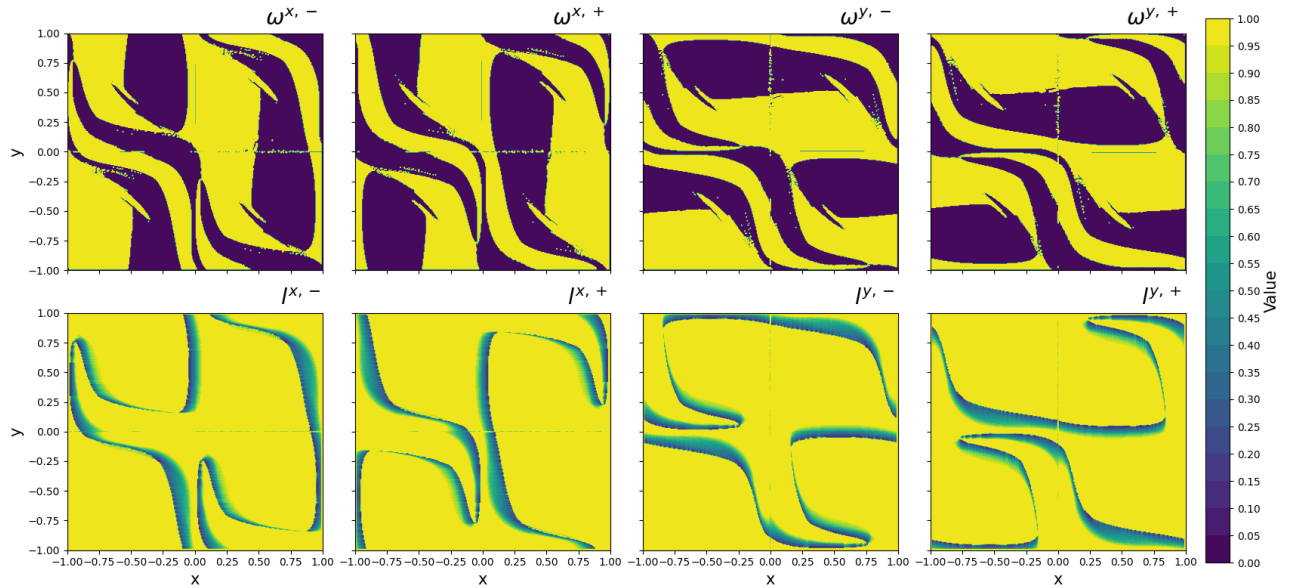


Figure 13: The visualizations of the values of  $\omega$  and  $l$  at time  $T = 0.4$  obtained using the ENO (4GS) scheme for the smooth initial conditions (42),  $M = 320$ ,  $C_{max} = 10$ .



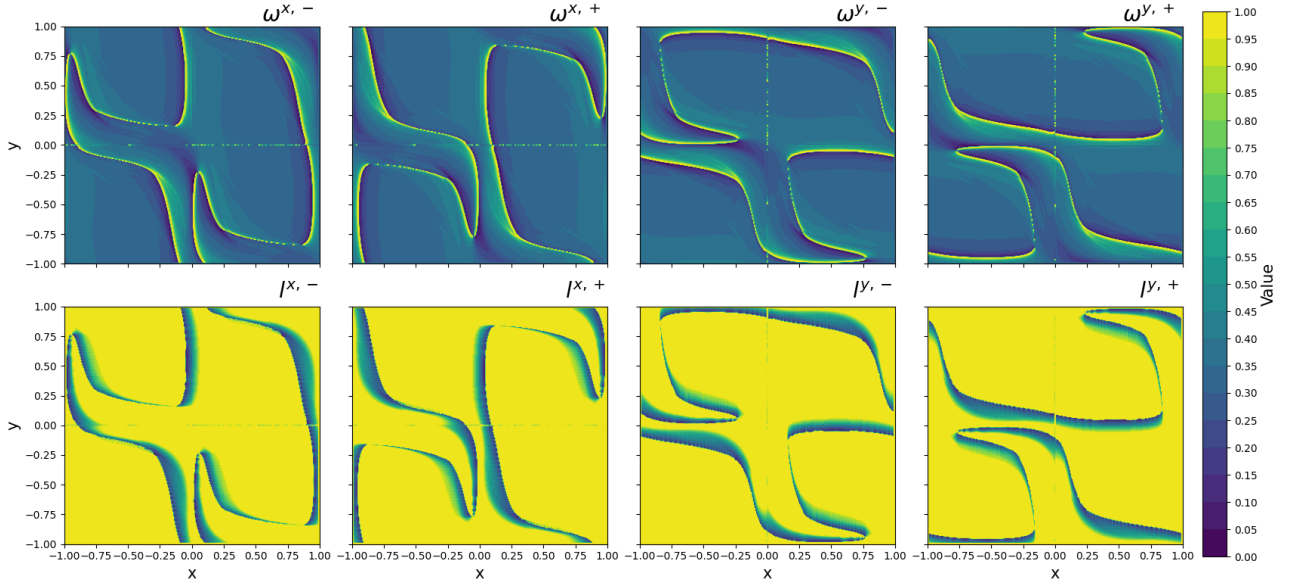


Figure 14: The visualizations of the values of  $\omega$  and  $l$  at time  $T = 0.4$  obtained using the WENO (4GS) scheme with the initial condition (42),  $M = 320$ ,  $C_{max} = 10$ .

The second problem is, again, defined for  $x, y \in [-1, 1]$  and will consider a rarefaction wave effect. The initial condition, see Figure 15, is given in the form

$$u^0(x, y) = \begin{cases} u_L & \text{if } \frac{x+y}{2} < 0 \\ u_R & \text{otherwise} \end{cases}, \quad (44)$$

for  $u_L = -1$  and  $u_R = 1$ ; and, the exact solution is prescribed as

$$u(x, y, t) = \begin{cases} u_L & \text{if } \frac{x+y}{2} \leq -t \\ \frac{x+y}{2t} & \text{if } -t < \frac{x+y}{2} \leq t \\ u_R & \text{if } \frac{x+y}{2} > t \end{cases}, \quad (45)$$

and we compute the solution for  $t \in [0, 0.4]$ .

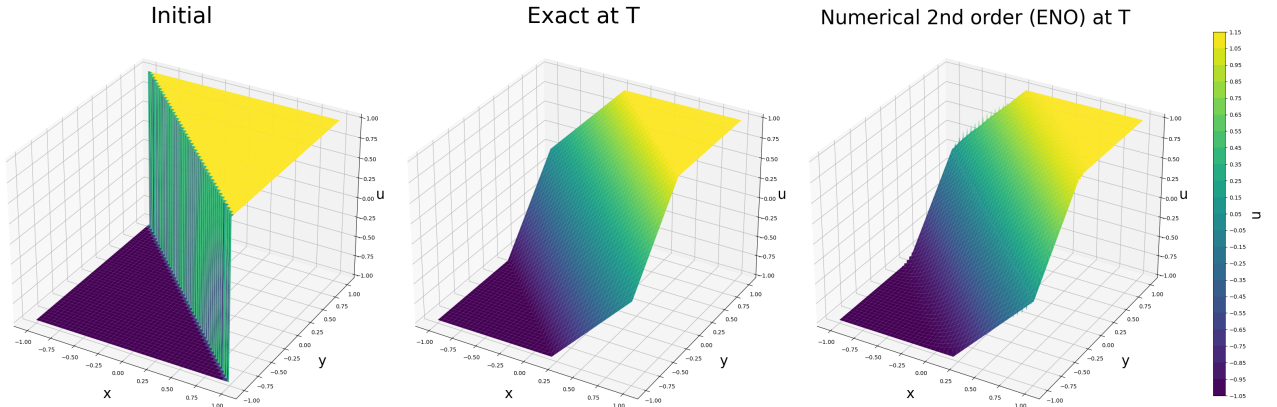


Figure 15: The initial condition (left), the exact solution (middle) and the numerical solution (right) obtained by the ENO (8GS) scheme at  $T = 0.4$ ,  $M = 320$  for the nonlinear problem with the initial condition (45).

This time we choose  $N = M/40$  number of time steps for  $M = 80, 160, 320, 640$ , with the value  $C_{max} = 8$ . The ENO and WENO (with  $\bar{\omega} = 1/3$ ) schemes were used to compute the solution, together with the first order accurate scheme, to demonstrate the difference in the errors obtained for 4 and 8 GS iterations, see Table 5.

		ENO, 4GS		WENO, 4GS		ENO, 8GS		WENO, 8GS		1st order	
$M$	$N$	E	EOC	E	EOC	E	EOC	E	EOC	E	EOC
80	2	0.34522	-	0.33213	-	0.33366	-	0.30509	-	0.49101	-
160	4	0.18866	0.87	0.17907	0.89	0.18425	0.85	0.16846	0.85	0.35488	0.46
320	8	0.09926	0.92	0.09331	0.94	0.09734	0.92	0.08890	0.92	0.24549	0.53
640	16	0.05096	0.96	0.04756	0.97	0.05008	0.95	0.04565	0.96	0.16124	0.60

Table 5: The numerical errors and the EOCs for the first and second (ENO, WENO) order accurate schemes for the nonlinear problem with the initial condition shown in Figure 15,  $T = 0.4$ ,  $C_{max} = 8$ .

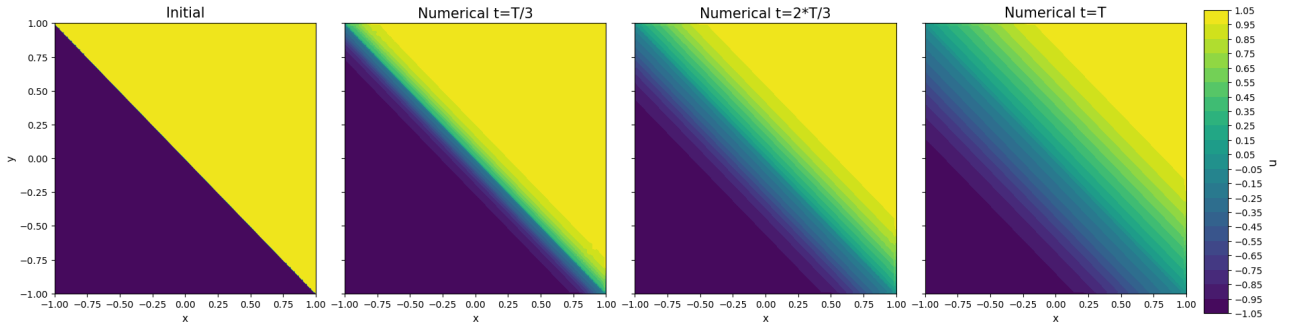


Figure 16: Numerical solution at three time steps  $t = 0, T/3, 2T/3, T$ , for  $T = 0.4$  obtained using the second order ENO (8GS) scheme,  $M = 320$ ,  $C_{max} = 8$ .

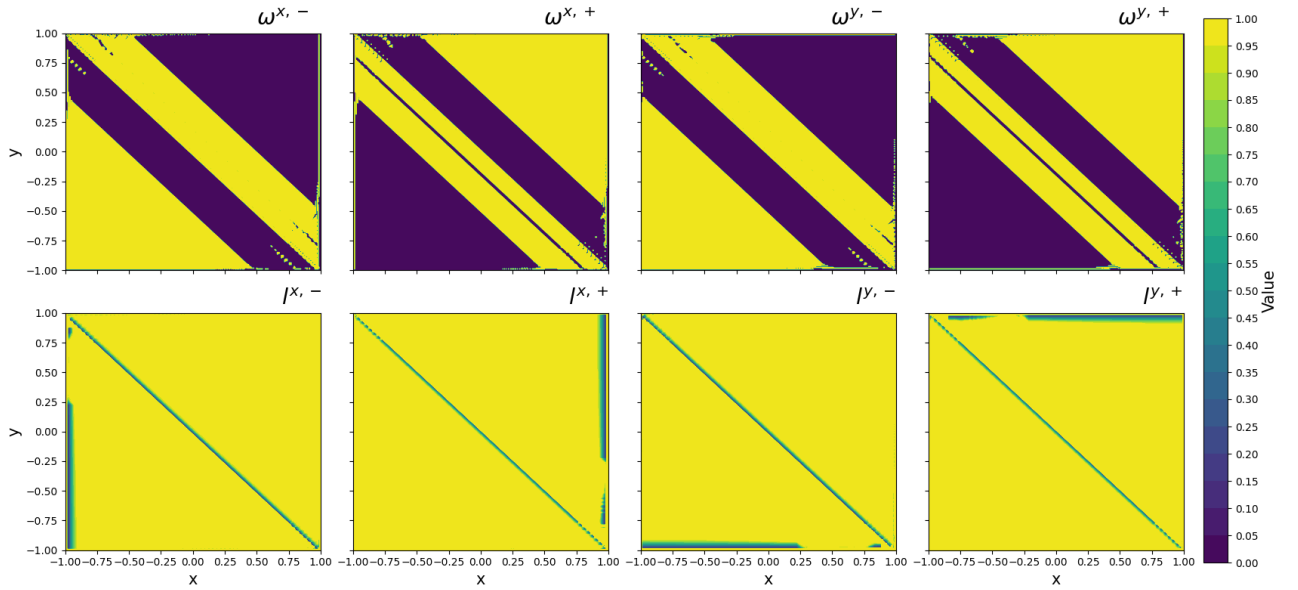


Figure 17: The visualizations of the values of  $\omega$  and  $l$  at time  $T = 0.4$  obtained using the ENO (8GS) scheme,  $M = 320$ ,  $C_{max} = 8$ .

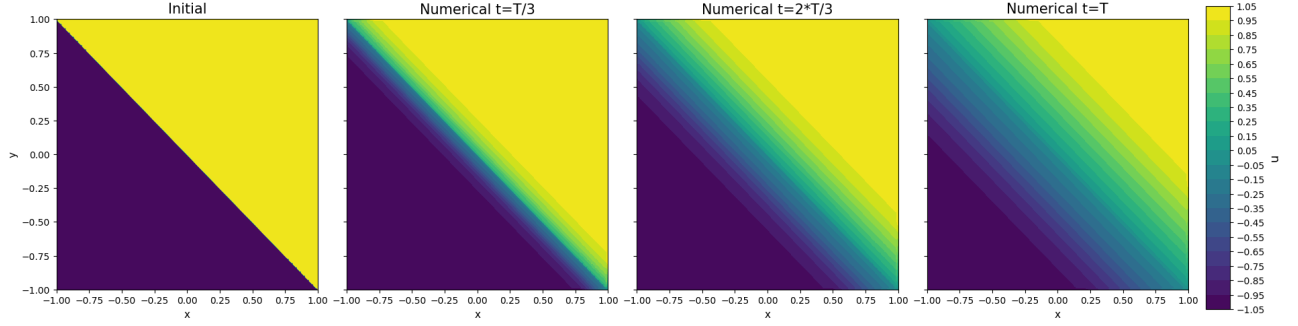


Figure 18: Numerical solution at three time steps  $t = 0, T/3, 2T/3, T$ , for  $T = 0.4$  obtained using the second order WENO (8GS) scheme,  $M = 320$ ,  $C_{max} = 8$ .

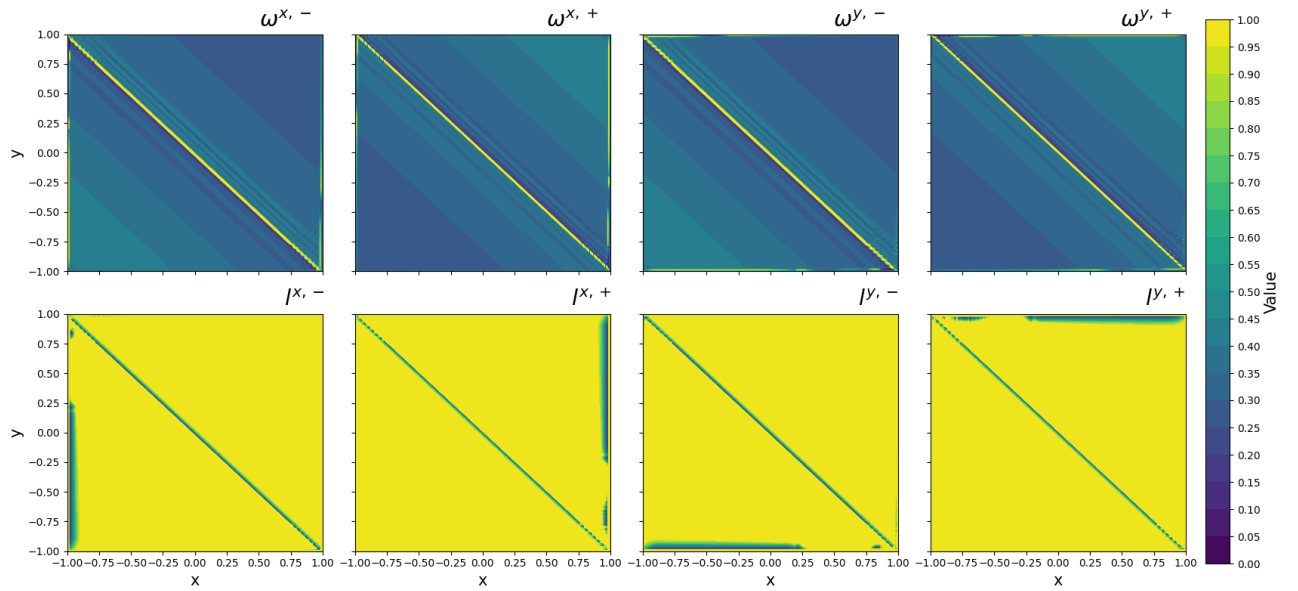


Figure 19: The visualizations of the values of  $\omega$  and  $l$  at time  $T = 0.4$  obtained using the WENO (8GS) scheme,  $M = 320$ ,  $C_{max} = 8$ .

The last problem deals with a discontinuity in the form of a shock wave and is defined for  $x, y \in [-1, 1]$  with the computational time  $t \in [0, 0.4]$ . The initial condition in Figure 20 is given in the form

$$u^0(x, y) = \begin{cases} u_{L1} & \text{if } x < -0.8 \text{ or } y < -0.8 \text{ or } x + y < -0.8 \\ u_{L2} & \text{if } x < 0.2 \text{ or } y < 0.2 \text{ or } x + y < 0.7 \\ u_{R2} & \text{otherwise} \end{cases}, \quad (46)$$

with  $u_{L1} = 1$ ,  $u_{R1} = u_{L2} = 0.1$  and  $u_{R2} = -0.5$ , and the exact solution is prescribed as

$$u(x, y, t) = \begin{cases} u_{L1} & \text{if } x < -0.8 + s_{x1}t \text{ or } y < -0.8 + s_{y1}t \text{ or } x + y < -0.8 + (s_{x1} + s_{y1})t \\ u_{L2} & \text{if } x < 0.2 + s_{x2}t \text{ or } y < 0.2 + s_{y2}t \text{ or } x + y < 0.7 + (s_{x2} + s_{y2})t \\ u_{R2} & \text{otherwise} \end{cases}, \quad (47)$$

with  $s_{x1}, s_{x2}, s_{y1}$  and  $s_{y2}$  being the shock speeds

$$\begin{aligned} s_{x1} &= \frac{f(u_{L1}) - f(u_{R1})}{u_{L1} - u_{R1}}, & s_{x2} &= \frac{f(u_{L2}) - f(u_{R2})}{u_{L2} - u_{R2}}, \\ s_{y1} &= \frac{g(u_{L1}) - g(u_{R1})}{u_{L1} - u_{R1}}, & s_{y2} &= \frac{g(u_{L2}) - g(u_{R2})}{u_{L2} - u_{R2}}. \end{aligned} \quad (48)$$

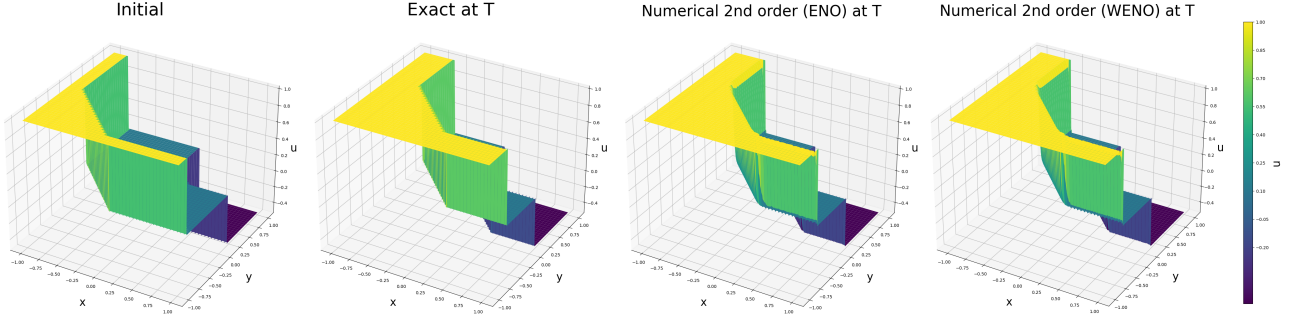


Figure 20: The visualization of the initial condition (left), the exact solution (second left) and the the numerical solutions (right) obtained by the ENO and WENO (8GS) schemes at  $T = 0.4$ ,  $M = 320$  for the nonlinear problem with the initial condition (46).

Again, we choose  $N = M/40$  number of time steps for  $M = 80, 160, 320, 640$ , with the value  $C_{max} = 8$ . The ENO and WENO ( $\bar{\omega} = 1/3$ ) schemes were used to compute the solution, using 4 and 8 GS iterations, together with the first order accurate scheme, to demonstrate the difference in the errors obtained, see Table 6. This time, it was useful to perform the eight Gauss-Seidel iterations, especially when using the ENO approximations, to obtain a better accuracy and convergence.

$M$	$N$	ENO, 4GS		WENO, 4GS		ENO, 8GS		WENO, 8GS		1st order	
		E	EOC	E	EOC	E	EOC	E	EOC	E	EOC
80	2	0.11936	-	0.11909	-	0.12562	-	0.12392	-	0.25841	-
160	4	0.06354	0.90	0.06341	0.90	0.06609	0.92	0.06534	0.92	0.15270	0.75
320	8	0.03547	0.84	0.03330	0.92	0.03411	0.95	0.03377	0.95	0.08418	0.85
640	16	0.02033	0.80	0.01721	0.95	0.01720	0.98	0.01704	0.98	0.04341	0.95

Table 6: The numerical errors and the EOCs for the first and second (ENO, WENO) order accurate schemes for the nonlinear problem with the initial condition shown in Figure 20,  $T = 0.4$ ,  $C_{max} = 8$ .

## 6 Conclusion

In this paper, we derived the second order accurate compact implicit finite volume numerical schemes in two dimensions for solving hyperbolic problems in the form of scalar conservation laws. Our approach utilizes the

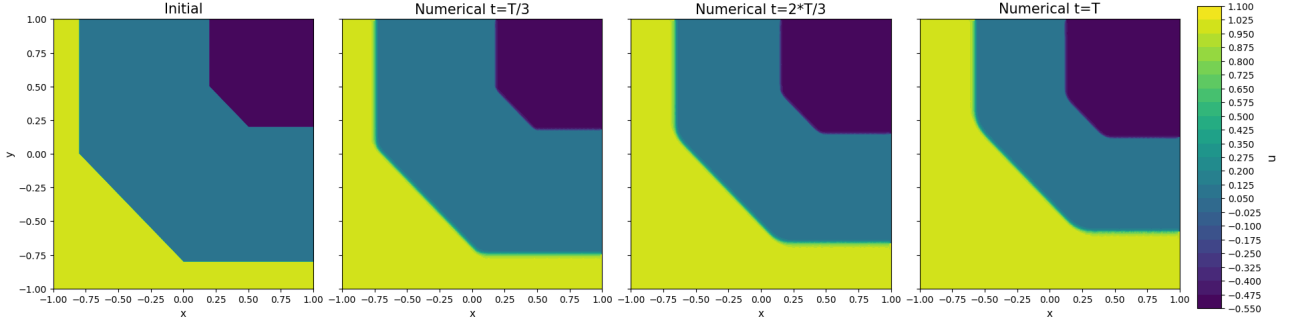


Figure 21: Numerical solutions at three times  $t = 0, T/3, 2T/3, T$  for  $T = 0.4$  obtained using the ENO (8GS) scheme for the example with shocks,  $M = 320$ ,  $C_{max} = 8$ .

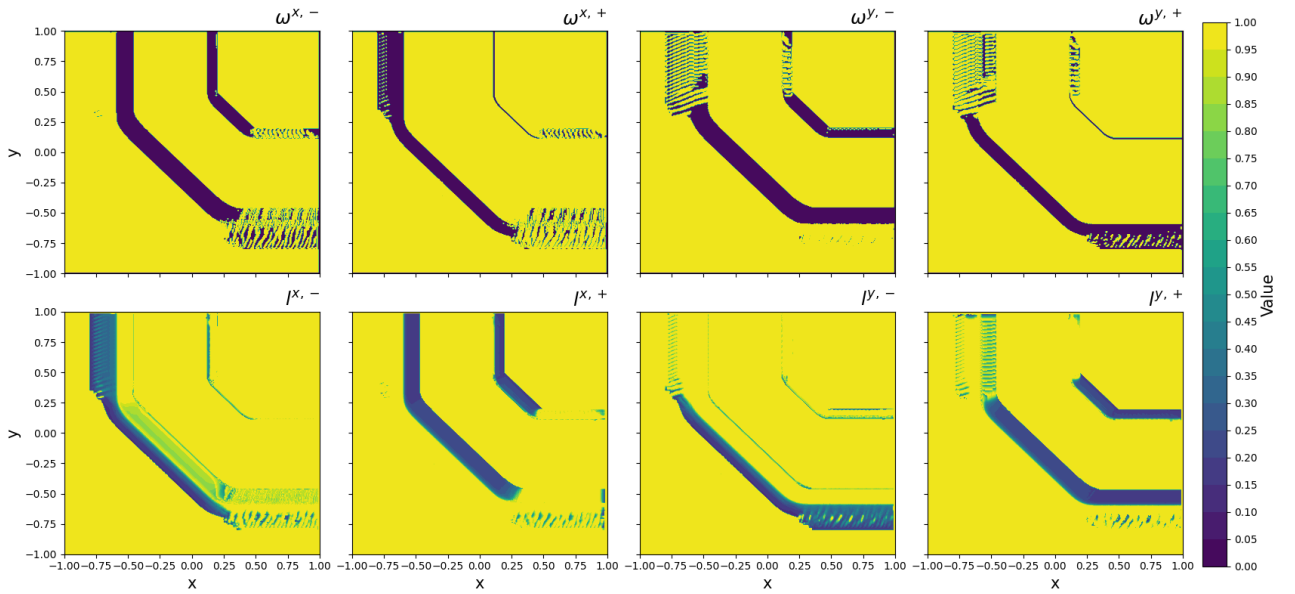


Figure 22: The visualizations of the values of  $\omega$  and  $l$  at time  $T = 0.4$  obtained using the ENO (8GS) scheme for the example with shocks,  $M = 320$ ,  $C_{max} = 8$ .

compactness of the stencil for computational efficiency as the solution of resulting algebraic systems can be efficiently obtained through the fast sweeping method combined with nonlinear Gauss-Seidel iterations.

The parametric form of the second order scheme inherently supports the use of Essentially Non-Oscillatory (ENO) and Weighted Essentially Non-Oscillatory (WENO) schemes for handling discontinuous solutions. By appropriately choosing the parameters in  $\omega$  and  $l$ , the approximation can be effectively limited in both space and time, mitigating oscillations in the numerical solutions through the corresponding predictor-corrector procedure.

We validated these schemes through numerical experiments on selected examples of linear and nonlinear scalar conservation laws demonstrating their properties in various scenarios.

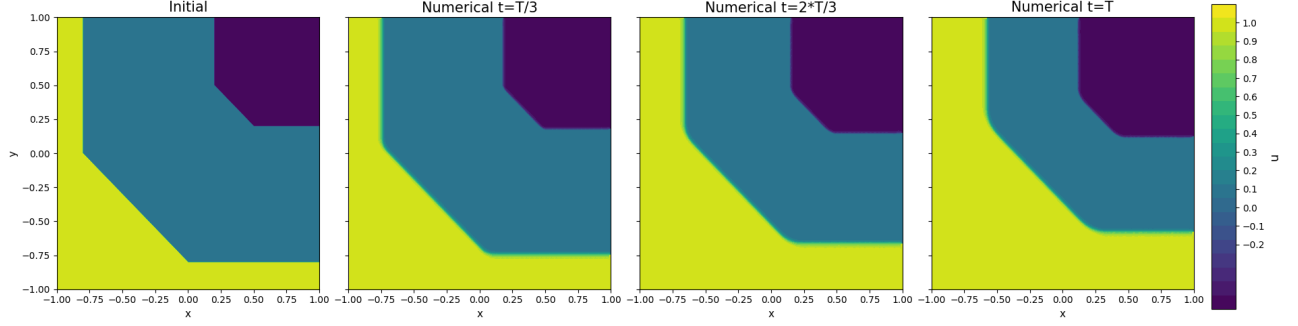


Figure 23: Numerical solutions at three times  $t = 0, T/3, 2T/3, T$ , for  $T = 0.4$  obtained using the WENO (8GS) scheme for the example with shocks,  $M = 320$ ,  $C_{max} = 8$ .

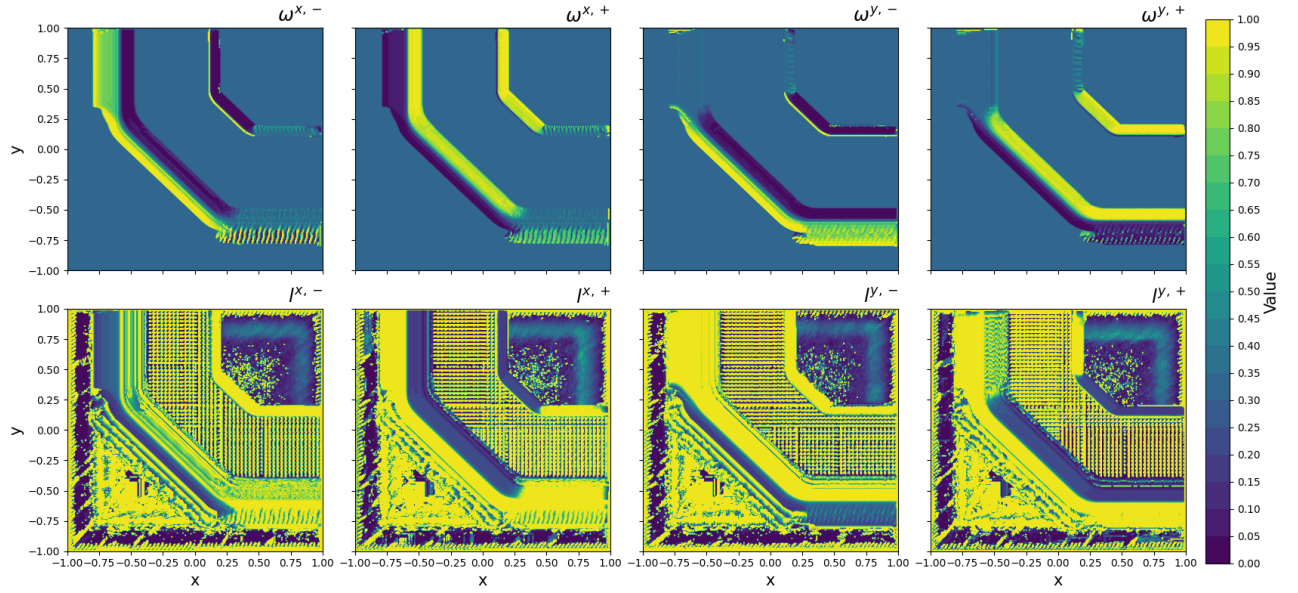


Figure 24: The visualizations of the values of  $\omega$  and  $l$  at time  $T = 0.4$  obtained using the WENO (8GS) scheme for the example with shocks,  $M = 320$ ,  $C_{max} = 8$ .

## References

- [1] Todd Arbogast et al. “A third order, implicit, finite volume, adaptive Runge–Kutta WENO scheme for advection–diffusion equations”. In: *Comput. Meth. Appl. Mech. Eng.* (2020), p. 113155.
- [2] Timothy Barth, Raphaële Herbin, and Mario Ohlberger. “Finite volume methods: foundation and analysis”. In: *Encyclopedia of computational mechanics second edition* (2018), pp. 1–60.
- [3] Philipp Birken and Viktor Linders. “Conservation Properties of Iterative Methods for Implicit Discretizations of Conservation Laws”. In: *J Sci Comput* 92.2 (2022), p. 60.
- [4] Sebastiano Boscarino et al. “High Order Semi-implicit WENO Schemes for All-Mach Full Euler System of Gas Dynamics”. In: *SIAM J. Sci. Comput.* (Apr. 2022), B368–B394.
- [5] Hugo Carrillo, Carlos Parés, and David Zorío. “Lax-Wendroff approximate Taylor methods with fast and optimized weighted essentially non-oscillatory reconstructions”. In: *Journal of Scientific Computing* (2021), p. 110358.
- [6] Sidafa Conde et al. “Implicit and Implicit–Explicit Strong Stability Preserving Runge–Kutta Methods with High Linear Order”. In: *J Sci Comput* 73.2 (2017), pp. 667–690.
- [7] Karthikeyan Duraisamy and James D. Baeder. “Implicit Scheme for Hyperbolic Conservation Laws Using Nonoscillatory Reconstruction in Space and Time”. In: *SIAM J. Sci. Comput.* 29.6 (2007), pp. 2607–2620.
- [8] Robert Eymard, Thierry Gallouët, and Raphaële Herbin. *Finite volume methods*. Vol. 7. Elsevier, 2000, pp. 713–1018.
- [9] Peter Frolkovič and Karol Mikula. “Semi-implicit second order schemes for numerical solution of level set advection equation on Cartesian grids”. In: *Appl. Num. Math.* (2018), pp. 129–142.
- [10] Peter Frolkovič and Michal Žeravý. “High Resolution Compact Implicit Numerical Scheme for Conservation Laws”. In: *Applied Mathematics and Computation* 442 (2023), p. 127720.
- [11] Peter Frolkovič et al. “Semi-Implicit Methods for Advection Equations with Explicit Forms of Numerical Solution”. In: *Japan J. Indust. Appl. Math.* 39.3 (2022), pp. 843–867.
- [12] I. Gómez-Bueno et al. “Implicit and Semi-Implicit Well-Balanced Finite-Volume Methods for Systems of Balance Laws”. In: *Applied Numerical Mathematics* 184 (2023), pp. 18–48.
- [13] Sigal Gottlieb et al. “High Order Strong Stability Preserving MultiDerivative Implicit and IMEX Runge–Kutta Methods with Asymptotic Preserving Properties”. In: *SIAM J. Numer. Anal.* 60.1 (Feb. 2022).
- [14] Friedemann Kemm. “A Comparative Study of TVD-limiters—Well-Known Limiters and an Introduction of New Ones”. In: *Int. J. Numer. Methods Fluids* 67.4 (2011), pp. 404–440.
- [15] Randall J Leveque. *Finite Volume Methods for Hyperbolic Problems*. en. 2nd. Cambridge UP, 2004.
- [16] Jiequan Li. “Two-stage fourth order: temporal-spatial coupling in computational fluid dynamics (CFD)”. In: *Adv. Aerodyn.* 1 (Feb. 2019), pp. 1–36.
- [17] Eduardo Lozano and Tariq D. Aslam. “Implicit fast sweeping method for hyperbolic systems of conservation laws”. In: *J. Comp. Phys.* 430 (Apr. 2021), p. 110039.
- [18] E. Macca and S. Boscarino. *Semi-Implicit-type Order-Adaptive CAT2 Schemes for Systems of Balance Laws with Relaxed Source Term*. 2023. arXiv: 2309.13954.
- [19] Victor Michel-Dansac and Andrea Thomann. “TVD-MOOD schemes based on implicit-explicit time integration”. In: *Applied Mathematics and Computation* (2022), p. 127397.
- [20] Lorenzo Pareschi and Giovanni Russo. “Implicit–explicit Runge–Kutta schemes and applications to hyperbolic systems with relaxation”. In: *Journal of Scientific Computing* 25.1 (2005), pp. 129–155.
- [21] G. Puppo, M. Semplice, and G. Visconti. “Quinpi: Integrating Conservation Laws with CWENO Implicit Methods”. In: *Commun. Appl. Math. Comput.* 5.1 (2022), pp. 343–369.
- [22] Gabriella Puppo, Matteo Semplice, and Giuseppe Visconti. “Quinpi: Integrating stiff hyperbolic systems with implicit high order finite volume schemes”. In: *arXiv preprint arXiv:2307.14685* (2023).
- [23] Jianxian Qiu and Chi-Wang Shu. “Finite Difference WENO Schemes with Lax–Wendroff-Type Time Discretizations”. In: *SIAM J. Sci. Comp.* 24.6 (2003), pp. 2185–2198.
- [24] G. van Rossum. *Python tutorial*. Tech. rep. Centrum voor Wiskunde en Informatica (CWI), May 1995.
- [25] David C. Seal, Yaman Güçlü, and Andrew J. Christlieb. “High-Order Multiderivative Time Integrators for Hyperbolic Conservation Laws”. In: *J. Sci. Comput.* 60 (2014), pp. 101–140.



- [26] Chi-Wang Shu. “Essentially non-oscillatory and weighted essentially non-oscillatory schemes for hyperbolic conservation laws”. In: *Advanced Numerical Approximation of Nonlinear Hyperbolic Equations*. Lecture Notes in Mathematics. Berlin, Heidelberg: Springer, 1998.
- [27] Angela Y. J. Tsai, Robert P. K. Chan, and Shixiao Wang. “Two-derivative Runge–Kutta methods for PDEs using a novel discretization approach”. In: *Numer. Alg.* 65 (2014), pp. 687–703.
- [28] Dagmar Žáková and Peter Frolkovič. “Higher Order Compact Implicit Finite Volume Schemes for Scalar Conservation Laws”. In: *Hyperbolic Probl. Theory Numer. Appl. Vol. II*. Ed. by Carlos Parés et al. Cham: Springer Nature Switzerland, 2024, pp. 221–231.
- [29] Jonas Zeifang and Jochen Schütz. “Implicit two-derivative deferred correction time discretization for the discontinuous Galerkin method”. In: *Journal of Computational Physics* 464 (2022), p. 111353.
- [30] Hongkai Zhao. “A fast sweeping method for eikonal equations”. In: *Math. Comput.* 74.250 (2005), pp. 603–627.
- [31] D. Zorío, A. Baeza, and P. Mulet. “An Approximate Lax–Wendroff-Type Procedure for High Order Accurate Schemes for Hyperbolic Conservation Laws”. In: *J. Sci. Comput.* 71 (2017), pp. 246–273.

## 7 Appendix

In this appendix, we formulate nonlinear conditions that the parameters  $\omega$  and  $\mathbf{l}$  in (25) and (26) must satisfy so that the high resolution scheme (16) for the linear advection equation (12) does not produce unphysical oscillations for divergence free velocity. For that purpose, we formulate the conditions when this scheme can be written in the form

$$P_{i,j}(u_{i,j}^{n+1} - u_{i,j}^n) + P_{i+1,j}(u_{i,j}^{n+1} - u_{i+1,j}^{n+1}) + P_{i-1,j}(u_{i,j}^{n+1} - u_{i-1,j}^{n+1}) \\ + P_{i,j+1}(u_{i,j}^{n+1} - u_{i,j+1}^{n+1}) + P_{i,j-1}(u_{i,j}^{n+1} - u_{i,j-1}^{n+1}) = 0, \quad (49)$$

where all five coefficients  $P$  are non-negative. Note that these coefficients are different for each discrete equation. Clearly, if (49) is valid, a local discrete minimum and maximum principle is fulfilled as  $u_{i,j}^{n+1}$  is a convex combination of all neighboring values. To express (16) in the form (49), all coefficients  $P$  must depend on unknown values of the numerical solution.

The first important assumption is that the discrete values of velocities must fulfill the discrete condition of incompressibility  $\nabla \cdot \vec{v} = 0$ , i.e.,

$$C_{i+1/2,j}^{x,+} + C_{i+1/2,j}^{x,-} - C_{i-1/2,j}^{x,+} - C_{i-1/2,j}^{x,-} + C_{i,j+1/2}^{y,+} + C_{i,j+1/2}^{y,-} - C_{i,j-1/2}^{y,+} - C_{i,j-1/2}^{y,-} = 0. \quad (50)$$

Using (50) multiplied by  $u_{i,j}^{n+1}$ , one can easily show that the first order scheme (17) of (16) can be transferred to the form (49) with

$$P_{i,j} = 1, \quad P_{i+1,j} = -C_{i+1/2,j}^{x,-}, \quad P_{i-1,j} = C_{i-1/2,j}^{x,+}, \quad P_{i,j+1} = -C_{i,j+1/2}^{y,-}, \quad P_{i,j-1} = C_{i,j-1/2}^{y,+}. \quad (51)$$

Consequently, if the parameters in  $\mathbf{l}$  are set to zero in (16), we obtain the first order form of the scheme that produces numerical solutions free of unphysical oscillations.

To subtract (50) multiplied by  $u_{i,j}^{n+1}$  from the high resolution scheme (16) with (25) and (26), we express

$$u_{i+1/2,j}^{n+1/2,-} - u_{i,j}^{n+1} = \frac{l_{i,j}^{x,-}}{2} \left( \omega_{i,j}^{x,-} + \frac{1 - \omega_{i,j}^{x,-}}{r_{i,j}^{x,-}} \right) (u_{i,j}^n - u_{i-1,j}^{n+1}) \quad (52)$$

$$u_{i+1/2,j}^{n+1/2,+} - u_{i,j}^{n+1} = - \left( u_{i,j}^{n+1} - u_{i+1,j}^{n+1} - \frac{l_{i+1,j}^{x,+}}{2} (\omega_{i+1,j}^{x,+} r_{i+1,j}^{x,+} + 1 - \omega_{i+1,j}^{x,+}) (u_{i,j}^n - u_{i+1,j}^{n+1}) \right) \quad (53)$$



and analogously for other terms with  $u_{i-1/2,j}^{n+1/2,\pm}$  and  $u_{i,j\pm 1/2}^{n+1/2,\pm}$ . In summary, we obtain the following equations,

$$\begin{aligned}
& u_{i,j}^{n+1} - u_{i,j}^n + C_{i+1/2,j}^{x,+} \frac{l_{i,j}^{x,-}}{2} (\omega_{i,j}^{x,-} + \frac{1 - \omega_{i,j}^{x,-}}{r_{i,j}^{x,-}}) (u_{i,j}^n - u_{i-1,j}^{n+1}) \\
& - C_{i+1/2,j}^{x,-} \left( u_{i,j}^{n+1} - u_{i+1,j}^{n+1} - \frac{l_{i+1,j}^{x,+}}{2} (\omega_{i+1,j}^{x,+} r_{i+1,j}^{x,+} + 1 - \omega_{i+1,j}^{x,+}) (u_{i,j}^n - u_{i+1,j}^{n+1}) \right) \\
& - C_{i-1/2,j}^{x,-} \frac{l_{i,j}^{x,+}}{2} (\omega_{i,j}^{x,+} + \frac{1 - \omega_{i,j}^{x,+}}{r_{i,j}^{x,+}}) (u_{i,j}^n - u_{i+1,j}^{n+1}) \\
& + C_{i-1/2,j}^{x,+} \left( u_{i,j}^{n+1} - u_{i-1,j}^{n+1} - \frac{l_{i-1,j}^{x,-}}{2} (\omega_{i-1,j}^{x,-} r_{i-1,j}^{x,-} + 1 - \omega_{i-1,j}^{x,-}) (u_{i,j}^n - u_{i-1,j}^{n+1}) \right) + \dots = 0, \tag{54}
\end{aligned}$$

where we have skipped analogous terms that should appear after  $C_{i,j\pm 1/2}^{y,\pm}$ . Taking into account that

$$u_{i,j}^n - u_{i\pm 1,j}^{n+1} = u_{i,j}^{n+1} - u_{i\pm 1,j}^{n+1} - (u_{i,j}^{n+1} - u_{i,j}^n),$$

the equations (54) can be written in the form (49) with the coefficients

$$P_{i-1,j} = C_{i+1/2,j}^{x,+} l_{i,j}^{x,-} A_{i,j}^{x,-} + C_{i-1/2,j}^{x,+} (1 - A_{i-1,j}^{x,-}), \quad P_{i+1,j} = -C_{i-1/2,j}^{x,-} l_{i,j}^{x,+} A_{i,j}^{x,+} - C_{i+1/2,j}^{x,-} (1 - A_{i+1,j}^{x,+}) \tag{55}$$

$$P_{i,j-1} = C_{i,j+1/2}^{y,+} l_{i,j}^{y,-} A_{i,j}^{y,-} + C_{i,j-1/2}^{y,+} (1 - A_{i,j-1}^{y,-}), \quad P_{i,j+1} = -C_{i,j-1/2}^{y,-} l_{i,j}^{y,+} A_{i,j}^{y,+} - C_{i,j+1/2}^{y,-} (1 - A_{i,j+1}^{y,+}) \tag{56}$$

$$\begin{aligned}
P_{i,j} = & 1 - C_{i+1/2,j}^{x,+} l_{i,j}^{x,-} A_{i,j}^{x,-} + C_{i-1/2,j}^{x,+} A_{i-1,j}^{x,-} + C_{i-1/2,j}^{x,-} l_{i,j}^{x,+} A_{i,j}^{x,+} - C_{i+1/2,j}^{x,-} A_{i+1,j}^{x,+} \\
& - C_{i,j+1/2}^{y,+} l_{i,j}^{y,-} A_{i,j}^{y,-} + C_{i,j-1/2}^{y,+} A_{i,j-1}^{y,-} + C_{i,j-1/2}^{y,-} l_{i,j}^{y,+} A_{i,j}^{y,+} - C_{i,j+1/2}^{y,-} A_{i,j+1}^{y,+}. \tag{57}
\end{aligned}$$

where the coefficients  $A$  are defined by

$$A_{i,j}^{x,\pm} := \frac{1}{2} \left( \omega_{i,j}^{x,\pm} + \frac{1 - \omega_{i,j}^{x,\pm}}{r_{i,j}^{x,\pm}} \right), \quad A_{i\pm 1,j}^{x,\pm} := \frac{l_{i\pm 1,j}^{x,\pm}}{2} (\omega_{i\pm 1,j}^{x,\pm} r_{i\pm 1,j}^{x,\pm} + 1 - \omega_{i\pm 1,j}^{x,\pm}) \tag{58}$$

and

$$A_{i,j}^{y,\pm} := \frac{1}{2} \left( \omega_{i,j}^{y,\pm} + \frac{1 - \omega_{i,j}^{y,\pm}}{r_{i,j}^{y,\pm}} \right), \quad A_{i,j\pm 1}^{y,\pm} := \frac{l_{i,j\pm 1}^{y,\pm}}{2} (\omega_{i,j\pm 1}^{y,\pm} r_{i,j\pm 1}^{y,\pm} + 1 - \omega_{i,j\pm 1}^{y,\pm}). \tag{59}$$

To prove the sign properties for the coefficients  $P$ , we are inspired by limiter techniques that exist in many variants [14, 10]. We follow the simplest and robust approach without an attempt to optimize the definitions of  $\omega$  and  $l$  to maximize accuracy.

Firstly, we require  $l_{i,j}^{*,\pm} = 0$  if  $r_{i,j}^{*,\pm} < 0$  with  $*$  =  $x$  and  $*$  =  $y$ . Note that the ratios in  $r$  take negative values only near extrema of numerical solutions. Having this requirement, it is enough to consider only positive values of ratios in  $r$ . In such case, to have non-negative coefficients  $P_{i\pm 1,j}$  and  $P_{i,j\pm 1}$  for any values of parameters in  $l$  in the interval  $[0, 1]$ , it is enough to require

$$A_{i\pm 1,j}^{x,\pm} \leq 1, \quad A_{i,j\pm 1}^{y,\pm} \leq 1. \tag{60}$$

The inequalities (60) are satisfied trivially by the ENO method (30) for positive values in  $r$ .

Finally, to prove the sign property for  $P_{i,j}$ , we have to use the parameters  $l_{i,j}^{*,\pm}$ . Note that for positive ratios in  $r$ , the coefficients  $A_{i,j}^{*,\pm}$ ,  $A_{i\mp 1,j}^{x,\pm}$ , and  $A_{i,j\mp 1}^{y,\pm}$  are non-negative. Using the definition of the parameter  $C$  in (29), we can estimate

$$\begin{aligned}
P_{i,j} \geq & 1 - C l_{i,j}^{x,-} A_{i,j}^{x,-} + C_{i-1/2,j}^{x,+} A_{i-1,j}^{x,-} - C l_{i,j}^{x,+} A_{i,j}^{x,+} - C_{i+1/2,j}^{x,-} A_{i+1,j}^{x,+} \\
& - C l_{i,j}^{y,-} A_{i,j}^{y,-} + C_{i,j-1/2}^{y,+} A_{i,j-1}^{y,-} - C l_{i,j}^{y,+} A_{i,j}^{y,+} - C_{i,j+1/2}^{y,-} A_{i,j+1}^{y,+}, \tag{61}
\end{aligned}$$

so to obtain  $P_{i,j} \geq 0$  we can require (if  $C > 1$ )

$$\begin{aligned}
& l_{i,j}^{x,-} A_{i,j}^{x,-} + l_{i,j}^{x,+} A_{i,j}^{x,+} + l_{i,j}^{y,-} A_{i,j}^{y,-} + l_{i,j}^{y,+} A_{i,j}^{y,+} \leq \\
& \frac{1}{C} \left( 1 + C_{i-1/2,j}^{x,+} A_{i-1,j}^{x,-} - C_{i+1/2,j}^{x,-} A_{i+1,j}^{x,+} + C_{i,j-1/2}^{y,+} A_{i,j-1}^{y,-} - C_{i,j+1/2}^{y,-} A_{i,j+1}^{y,+} \right). \tag{62}
\end{aligned}$$

Clearly, there are many ways how to define the parameters  $\mathbf{l}$ , in theory, to satisfy (62). For any such definition, the high resolution scheme (16) will represent nonlinear system of algebraic equations. In our current approach given by (28), we use iterative methods in the form of predictor-corrector scheme together with dimensional splitting and fast sweeping method. We plan to develop more involved definitions of parameters  $\mathbf{l}$  in future.